SUPPLEMENTAL MATERIAL: SYNTHETIC $\mathbb{Z}_2$ GAUGE THEORIES BASED ON PARAMETRIC EXCITATIONS OF TRAPPED IONS

Supplementary Note 1: Background gauge fields and trapped ions

Parametric tunnelling and synthetic dimensions

Given the importance of the idea of parametric tunnelling for the quantum simulation schemes of dynamical gauge theories presented in the main text, we present in this Appendix a detailed discussion, an its application to ion crystals. We start in a general setup by considering a set of bosonic/fermionic particles that can be created and annihilated by operators $a_d^\dagger, a_d$ with the corresponding commutation/anti-commutation algebra, where $d \in \mathscr{D}$ labels a specific degree of freedom of these particles. In the context of quantum many-body models and lattice field theories, the indexing set $\mathscr{D}$ typically contains the positions of a microscopic lattice in which the particles can reside, as already mentioned in the introduction. In this context, the geometry of the lattice determines the kinetic energy of the microscopic Hamiltonian, which is described by a tunnelling term $t_{dd'} a_d^\dagger a_{d'}$, where $t_{dd'}$ is the hopping matrix element between a pair of sites labeled by $d \neq d'$. Typically, these tunnelings decay very fast with the distance, and one only considers nearest neighbours, such that the connectivity of the lattice, i.e. the edges/links of a graph, gets directly in-built in the tunnelling matrix. Additionally, in condensed matter, $d \in \mathscr{D}$ can contain other internal degrees of freedom, e.g. spin of the valence electrons. In the context of synthetic dimensions, it is these extra degrees of freedom that provide us with a new means to engineer a synthetic dimension.

The idea of synthetic dimensions is that the effective connectivity of the tunnelling matrix can be externally designed by introducing additional periodic drivings. These, in fact, induce new couplings that can be interpreted as effective edges/links even when the corresponding degrees of freedom are not related to any Bravais lattice at all. A possible scheme uses a parametric tunnelling, as illustrated now with a simple example. We consider two modes $d \in \mathscr{D} = \{1,2\}$ of energies ω_d ($\hbar = 1$ henceforth), such that the bare Hamiltonian is

$$H_0 = \omega_1 a_1^\dagger a_1 + \omega_2 a_2^\dagger a_2. \tag{73}$$

One now adds the following parametric excitation

$$V(t) = \Omega_\mathrm{d} a_2^\dagger a_1 \cos(\phi_\mathrm{d} - \omega_\mathrm{d} t) + \mathrm{H.c.}, \tag{74}$$

where Ω_d, ω_d, and ϕ_d are the amplitude, frequency, and phase of the drive, respectively. In the parametric regime, i.e.,

$$\omega_\mathrm{d} = \omega_2 - \omega_1, \quad |\Omega_\mathrm{d}| \ll 4|\omega_2 - \omega_1|, \tag{75}$$

one can show that an effective tunnelling term between both modes is induced by the drive. Going to the interaction picture with respect to Eq. (73), it is straightforward to recognise that the resonance condition of Eq. (75) provides the required energy to bridge the gap between the modes and couple them. Additionally, when the driving amplitude is constrained by Eq. (75), a rotating-wave approximation shows that the mode coupling $V_\mathrm{I}(t) \approx H_\mathrm{eff}$ becomes a time-independent effective Hamiltonian with a simple frequency-conversion term

$$H_\mathrm{eff} = t_{1,\mathbf{e}_1} a_2^\dagger a_1 + \mathrm{H.c.}, \quad \text{with } t_{1,\mathbf{e}_1} = \frac{\Omega_\mathrm{d}}{2} \mathrm{e}^{\mathrm{i}\phi_\mathrm{d}}. \tag{76}$$

In the context of synthetic dimensions, one finds that a non-zero tunnelling has been established, which could be understood as a new connectivity link of a synthetic lattice. This tunnelling $t_{1,\mathbf{e}_1}$ is labelled by the synthetic lattice site index 1 from which the particle departs, and the unit link vector $\mathbf{e}_1$ that connects it to the lattice site 2, into which the particle tunnels. In this simple case, accordingly, the synthetic lattice is just composed of two sites labelled by the indexes of the mode frequencies. We note that, for a single link, the complex phase of the tunnelling is trivial and has no dynamical consequences, i.e. it can be readily gauged away by a local $U(1)$ transformation acting on the modes. However, this parametric scheme can be generalised to a larger set $\mathscr{D}$, in which the complex phase of the effective tunnelling (76) may have non-trivial consequences. As discussed in [170, 172], one can create synthetic lattices in a way that, when the particle tunnels around a closed path γ, it gains a non-zero phase $\sum_{\ell\in\gamma}\phi_\ell = \Phi_\mathrm{AB}$ that simulates a synthetic Aharonov-Bohm phase. Even if the particles have a vanishing charge, their tunnelling resembles that of a charged particle in an external magnetic field via the so-called Peierls' substitution [287], which originally concerned electrons in a narrow-band material subjected to a perpendicular magnetic field [288]. The quadratic lattice models with Peierls' phases provide a playground for studying the integer quantum Hall effect and topological band theory [289]. We discuss this point in detail below.

Peierls ladders with trapped-ion chains

So far, we have not yet discussed how the parametric term (74) can be created and controlled in a specific physical system. The parametric scheme has been implemented in arrays of superconducting circuits [172] but, to the best of our knowledge, its realisation in trapped-ion crystals has not been discussed so far. We now describe how to exploit this method to build a quantum simulator of a bosonic quantum Hall ladder using the transverse vibrations of a chain of N trapped ions in a linear Paul trap [290]. This will prepare the ground for the scheme of dynamical $\mathbb{Z}_2$ gauge fields discussed in the main text, which exploit similar concepts with a new twist.

Following [244–246], for a linear Paul trap with trap frequencies $\omega_z \ll \omega_x, \omega_y$, the ions form a linear chain along the z-axis (see Supplementary Figure 1). The transverse vibrations of each ion [291] around its equilibrium position are described by

$$H_0 = \sum_d \omega_d a_d^\dagger a_d + \sum_{d\neq d'} t_{dd'} a_d^\dagger a_{d'}. \tag{77}$$

Here, the labelling index reads $d = (i,\alpha) \in \mathscr{D}$, and the set $\mathscr{D}$ contains the label for the ions in the chain $i \in \{1,\cdots,N\}$,

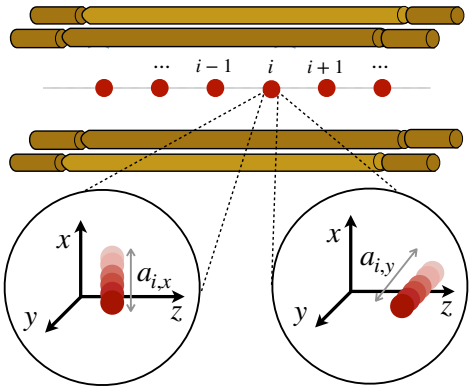

Supplementary Figure 1. **Transverse vibrational excitations:** Schematic representation of an ion chain in a linear Paul trap. In the insets, we represent the transverse local vibrational excitations of a single ion in the chain.

and the label for the two possible directions of the vibrations transverse to the chain $\alpha \in \{x,y\}$. In addition, $a_d^\dagger, a_d$ are the bosonic creation-annihilation operators for the corresponding local vibrations around the equilibrium positions of the ions $\boldsymbol{r}_i^0$, which we have assumed to be aligned along the null of the radio-frequency (rf) pseudo-potential of the linear Paul trap, such that excess micromotion can be neglected [292]. Additionally, the modulation frequencies to be introduced below must be much lower than the rf driving of the trap to also neglect the intrinsic quantum-mechanical micromotion [293]. As discussed in [246], the expansion of the Coulomb interaction to second order leading to Eq. (77) does not mix the x,y modes, and one finds that the tunnelling matrix decay with the inter-ion distance following a dipolar law

$$t_{(i,\alpha)(j,\beta)} = \frac{1}{2m\omega_\alpha}\frac{e^2}{8\pi\varepsilon_0|\boldsymbol{r}_i^0-\boldsymbol{r}_j^0|^3}\delta_{\alpha,\beta}, \tag{78}$$

where m is the ion mass, ε_0 the vacuum permittivity, and $\delta_{\alpha,\beta}$ is the Kronecker delta. The on-site energies are related to the effective trap frequencies ω_α of the time-averaged pseudo-potential [291] by the following expression

$$\omega_{i,\alpha} = \omega_\alpha - \sum_{j\neq i}\frac{1}{2m\omega_\alpha}\frac{e^2}{8\pi\varepsilon_0|\boldsymbol{r}_i^0-\boldsymbol{r}_j^0|^3}. \tag{79}$$

Since the Hamiltonian of Eq. (77) has a global $U(1)\times U(1)$ symmetry under $a_d \mapsto \mathrm{e}^{\mathrm{i}\varphi}a_d$, $a_d^\dagger \mapsto \mathrm{e}^{-\mathrm{i}\varphi}a_d^\dagger$, the total number of transverse vibrational excitations along each trap axis is individually conserved. Although phonons in crystals typically refer to the excitations of the collective vibrational modes, it is customary to refer to these local vibrational modes also as phonons in the trapped-ion community, and we have followed this convention in the main text. The novelty with respect to the crystal phonons underlying the transverse sound waves in elastic solids [294] is that, since the phonon number is conserved when $|t_{dd'}| \ll 2\omega_\alpha$ [291], we can thus think of these transverse vibrational excitations as particles localised to each of the ions. Just like electrons on a solid, the phonons tend to spread over the chain due to the dipolar tunnelling of Eq. (78). We note that the dynamics of these local phonons due to the effective tight-biding Hamiltonian of Eq. (77) has been observed in various trapped-ion experiments [180, 295–302].

Let us now discuss how to exploit parametric excitations to realise synthetic phonon ladders subjected to an effective background gauge field. There have been some prior works on trapped-ion parametric drivings which, to the best of our knowledge, have focused on rather different goals. For instance, in [303], parametric modulations are used to design cooling and detection methods for the spectroscopy of a single trapped electron and proton, as well as for squeezing and linear amplification. The former requires a parametrically-modulated quadrupole potential that couples two different vibrational directions [304], whereas the latter employs a periodic modulation of the trap frequencies, and can thus be achieved by applying an additional oscillating potential to the rf trap electrodes. Parametric modulations can also be obtained optically, exploiting the cross-beam ac-Stark shift of a pair of far-detuned laser beams [224, 305]. Although the parametric modulations obtained through the electronic equipment have led to larger amplification in recent experiments [306], we stick to optical ones in our work, as they are more flexible for the generation of synthetic gauge fields.

Our goal is to interpret the transverse vibrational directions of Supplementary Figure 1 as a new synthetic "dimension". Note that, however, the x and y directions are decoupled at this quadratic order (Eq. (78)), such that the Hamiltonian of Eq. (77) describes two decoupled dipolar chains. We now discuss how a parametric excitation of the tunnelling can be induced, and how this term can be used to derive a model with couplings between the two chains, such that the global symmetry reduces to $U(1)\times U(1)\mapsto U(1)$, and only the total number of transverse vibrational quanta is conserved. We will see that, from this perspective, the phonons move in a synthetic two-leg ladder and, moreover, argue that they can also be subjected to an effective Peierls' phase mimicking the microscopic model for charged particles under external magnetic fields. We consider that each ion is illuminated by a global two-beam laser field, the beat note of which is far detuned from any electronic transition [224]. The ions, all prepared in the same internal state of the ground-state manifold [307], thus experience an ac-Stark shift that yields the following optical potential

$$V(t) = \sum_{n,n'=1,2}\sum_{i=1}^{N}\Omega_{n,n'}\mathrm{e}^{\mathrm{i}(\boldsymbol{k}_{\mathrm{L},n}-\boldsymbol{k}_{\mathrm{L},n'})\cdot\boldsymbol{r}_i-(\omega_{\mathrm{L},n}-\omega_{\mathrm{L},n'})t}+\mathrm{H.c.}. \tag{80}$$

Here, $\omega_{\mathrm{L},n}(\boldsymbol{k}_{\mathrm{L},n})$ is the frequency (wave-vector) of each beam $n\in\{1,2\}$ of the global laser field, and $\Omega_{n,n'} = -\Omega_{\mathrm{L},n}\Omega^*_{\mathrm{L},n'}/4\Delta$ is the ac-Stark shift arising from two-photon processes. In those processes, a photon is absorbed from the n-th beam by the i-th ion with the Rabi frequency $\Omega_{\mathrm{L},n}$ and a large detuning Δ, such that the ion is only virtually excited. Subsequently, the ion is de-excited to the same internal state by emitting a photon onto the n'-th beam [224].

In addition to the standard ac-Stark shifts in Eq. (80), i.e. terms with $n = n'$ that contribute with an energy shift $\Delta E_{\rm ac} = \sum_n \Omega_{n,n}$, one also obtains crossed beat note terms that lead to periodic modulations in space (time) when the laser wavevectors (frequencies) are not co-linear (equal). In this case, one defines the beat note wave-vector and frequency as $\boldsymbol{k}_{\rm d} = \boldsymbol{k}_{\rm L,1} - \boldsymbol{k}_{\rm L,2}$, and $\omega_{\rm d} = \omega_{\rm L,1} - \omega_{\rm L,2}$, respectively. Noting that the ion positions can be expanded in terms of the local phonon operators via $\boldsymbol{r}_i = \boldsymbol{r}_i^0 + \sum_\alpha \mathbf{e}_\alpha \frac{1}{\sqrt{2m\omega_\alpha}}(a_{i,\alpha} + a_{i,\alpha}^\dagger)$, where $\mathbf{e}_\alpha$ is the unit vector in the direction of the transverse ion vibration α, one can substitute and expand the optical potential (80) in the so-called Lamb-Dicke regime

$$\eta_\alpha = \boldsymbol{k}_{\rm d} \cdot \mathbf{e}_\alpha / \sqrt{2m\omega_\alpha} \ll 1. \tag{81}$$

The Taylor expansion of Eq. (80) then leads to a sum of terms with all possible powers of the phonon operators. By choosing the correct beat note frequency, it is possible to select which of them brings in the leading contribution. In particular, for

$$\omega_{\rm d} = \omega_y - \omega_x, \quad |\Omega_{\rm d}| \ll |\omega_y - \omega_x|, \tag{82}$$

where we assume that $|\omega_x - \omega_y| \ll \omega_x, \omega_y$, a rotating-wave approximation shows that the optical potential contains the desired parametric excitation of a tunnelling term that generalises Eq. (74) to an arbitrary number of lattice sites, namely

$$V(t) \approx \sum_i \Delta E_{\rm ac} + \sum_i \Omega_{\rm d} \cos(\phi_i - \omega_{\rm d} t) a_{i,y}^\dagger a_{i,x} + \text{H.c.}, \tag{83}$$

where we have introduced the parameters

$$\Omega_{\rm d} = |\Omega_{1,2}| \eta_x \eta_y, \quad \phi_i = \boldsymbol{k}_{\rm d} \cdot \boldsymbol{r}_i^0 + \arg(-\Omega_{1,2}). \tag{84}$$

Note that, due to the constraints in Eq. (82), we have neglected other contributions in the Lamb-Dicke expansion.

One can readily see that, in addition to the irrelevant ac-Stark shift $\Delta E_{\rm ac}$, we have obtained a parametric modulation like Eq. (74) that involves simultaneously all of the ions in the chain. Repeating the same arguments as in the simple two-mode case (Eq. (74)), one finds that the parametric drive can activate the tunnelling of a phonon along the new synthetic direction (see Supplementary Figure 2 **(a)**), such that the tunnelling matrix of Eq. (78) becomes $t_{dd'} \mapsto \tilde{t}_{dd'}$ with

$$\tilde{t}_{(i,\alpha)(j,\beta)} = t_{(i,\alpha)(j,\beta)} + \frac{\Omega_{\rm d}}{2} e^{i\varepsilon_{\alpha,\beta}\phi_j} \delta_{i,j}(1 - \delta_{\alpha,\beta}), \tag{85}$$

Here, in addition to the Kronecker delta, we have used the fully anti-symmetric tensor defined as $\varepsilon_{x,y} = -\varepsilon_{y,x} = 1$, $\varepsilon_{x,x} = \varepsilon_{y,y} = 0$. By making the following identification

$$a_{i,x}, a_{i,x}^\dagger \mapsto a_{i\mathbf{e}_1}, a_{i\mathbf{e}_1}^\dagger, \quad a_{i,y}, a_{i,y}^\dagger \mapsto a_{i\mathbf{e}_1+\mathbf{e}_2}, a_{i\mathbf{e}_1+\mathbf{e}_2}^\dagger, \tag{86}$$

we obtain, in the interaction picture, a tight-binding model for bosons in a synthetic two-leg ladder

$$H_{\rm eff} = \sum_{\boldsymbol{i}} \sum_{\boldsymbol{\ell} \in \mathscr{L}\{\boldsymbol{i}\}} t_{\boldsymbol{i},\boldsymbol{\ell}} a_{\boldsymbol{i}+\boldsymbol{\ell}}^\dagger a_{\boldsymbol{i}}. \tag{87}$$

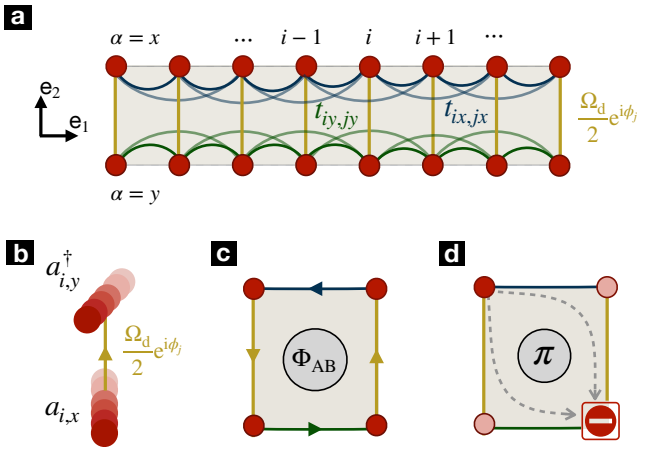

Supplementary Figure 2. **Synthetic dimensions in trapped-ion chains: (a)** Schematic representation of a synthetic Peierls ladder. The sites of the upper and lower legs of the ladder represent the local vibrations of the ions along the x and y transverse directions, respectively. The dipolar tunnelings (78) are represented by intra-leg links that connect distant ions. The resulting parametric tunnelings in Eq. (88) are depicted by the vertical inter-leg links, and correspond to the frequency-conversion process of **(b)**. **(c)** For a pair of ions, the effective rectangular plaquette can lead to a net Aharonov-Bohm phase $\Phi_{\rm AB}$ (89) for a phonon that tunnels along the corresponding synthetic links. **(d)** For $\Phi_{\rm AB} = \pi$, there can be perfect destructive interference for the phonon, which mimics the Aharonov-Bohm interference of an electron that travels around an infinitely-thin solenoid.

Here, a boson at the synthetic lattice site $\boldsymbol{i}$ can tunnel horizontally or vertically to the site $\boldsymbol{i}+\boldsymbol{\ell}$ along the synthetic links labelled by $\boldsymbol{\ell} \in \mathscr{L}\{\boldsymbol{i}\}$. The tunnelling amplitudes read

$$\begin{aligned} t_{i\mathbf{e}_1,\ell\mathbf{e}_1} &= \tilde{t}_{(i+\ell,x)(i,x)}, & t_{i\mathbf{e}_1,\mathbf{e}_2} &= \frac{\Omega_{\rm d}}{2} e^{+i\phi_i}, \\ t_{i\mathbf{e}_1+\mathbf{e}_2,\ell\mathbf{e}_1} &= \tilde{t}_{(i+\ell)(y;i,y)}, & t_{i\mathbf{e}_1+\mathbf{e}_2,-\mathbf{e}_2} &= \frac{\Omega_{\rm d}}{2} e^{-i\phi_i}. \end{aligned} \tag{88}$$

In comparison to the parametric tunnelling of Eq. (74), which also leads to a tunnelling strength with a complex phase (see Eq. (76)), we see that the current scheme leads to a site-dependent phase as a consequence of the spatial modulation of the optical potential (80), as depicted in Supplementary Figure 2**(b)**. This inhomogeneity can be exploited, as depicted in Supplementary Figure 2 **(c)**, to induce an effective Peierls' phase, such that the phonons in the synthetic ladder mimic the dynamics of electrons under a magnetic field. In fact, if the local phonon tunnels around the smallest rectangular plaquette $t_{i\mathbf{e}_1,\mathbf{e}_1} t_{(i+1)\mathbf{e}_1,\mathbf{e}_2} t_{(i+1)\mathbf{e}_1+\mathbf{e}_2,-\mathbf{e}_1} t_{i\mathbf{e}_1+\mathbf{e}_2,-\mathbf{e}_2} \propto e^{i\Phi_{\rm AB}}$, it gains a net phase that can no longer be gauged away as in the simple two-mode case of Eq. (76). In fact, this phase is analogous to the Aharonov-Bohm phase [169] for electrons moving in a plane under a perpendicular magnetic field

$$\Phi_{\rm AB} = \boldsymbol{k}_{\rm d} \cdot (\boldsymbol{r}_{i+1}^0 - \boldsymbol{r}_i^0) =: 2\pi \frac{\Phi_B}{\Phi_0}, \tag{89}$$

where $\Phi_B = \int_\square \mathrm{d}\boldsymbol{S} \cdot \boldsymbol{B}_{\rm bg}$ is the flux of an effective magnetic field $\boldsymbol{B}_{\rm bg}$ across the plaquette $\square$, and $\Phi_0 = h/e$ is the quan-

tum of flux. As a consequence of this flux, which can be controlled by tilting the laser wave-vector with respect to the ion chain, one could for instance observe Aharonov-Bohm destructive interference for $\Phi_{AB} = \pi$, in which a single phonon cannot tunnel two sites apart along a synthetic plaquette (see Supplementary Figure 2 **(d)**). Let us note that this Aharonov-Bohm interference occurs at the level of phonons, which have a zero net charge, and thus differs from the interference of charged ions tunnelling between two different crystalline configurations, neatly observed in experiments with a real magnetic field [308].

For larger ion crystals, the analogy with a homogeneous magnetic field is still valid in spite of the existence of dipolar tunnelings, provided that the equilibrium positions of the ions are equally spaced. The equal spacing can be achieved by designing arrays of individual traps with micro-fabricated surface-electrode traps [247–259], by introducing anharmonic confining potentials in segmented ion traps [309–313], or in ring traps [314, 315]. Let us note that, even if one achieved an homogeneous spacing, the longer-range nature of the tunnelings imply that the excitations can now enclose larger plaquettes potentially changing the interference phenomena. In the pi-flux case, the next-to-nearest neighbour tunnelling leads to plaquettes with zero flux, which may challenge the existence of the perfect destructive interference of Supplementary Figure 2 **(d)**. Nevertheless, these larger plaquettes are enclosed at a considerably slower pace, as the tunnelling strengths decay with the cube of the distance (78). We have numerically observed that an almost perfect Aharonov-Bohm interference can still occur when considering how a phononic excitation travels between opposite corners of the synthetic ladder [316].

Let us close this Appendix by highlighting that the effective magnetic field underlying Eq. (89) is not a true dynamical magnetic field, but rather a fixed background field. One can indeed push the analogy to the level of the vector potential using $\boldsymbol{B}_{\rm bg} = \boldsymbol{\nabla} \times \boldsymbol{A}_{\rm bg}$, but the $U(1)$ gauge field $\boldsymbol{A}_{\rm bg}$ would still be a background field, the dynamics of which can only be fixed externally, and has nothing to do with Maxwell electrodynamics. In the main text, we describe how this scheme of parametric tunnelings can be generalised to get closer to this situation, and be able to explore lattice gauge theories.

Supplementary Note 2: Dynamical gauge fields and trapped ions

Dipole light-shift scheme

In this Appendix, we consider a $^{88}Sr^{+}$ ion confined in the setup presented in Refs. [228, 229], an provide a more detailed discussion of the specific experimental parameters, and the errors that arise in the analog scheme for the $\mathbb{Z}_2$ gauge link QS. The secular frequency of the axial in-phase mode can be set to $\omega_z/2\pi = 1.2\,$MHz, while the radial secular frequency is $\omega_x/2\pi = 1.9\,$MHz. The qubit states $|\uparrow_1\rangle, |\downarrow_1\rangle$ can be defined by two ground state levels of the $5S_{1/2}$ manifold shown in Supplementary Figure 3. For such a ground state qubit, the light shifts are created by a far-detuned dipole-mediated

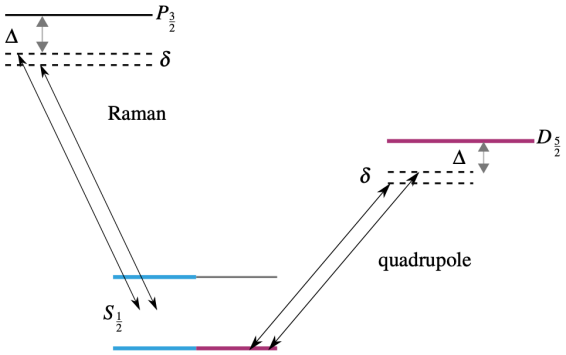

Supplementary Figure 3. **Beam configurations for the light-shift scheme:** We consider the ground state qubit (cyan lines) and the optical qubit (magenta) in $^{88}Sr^{+}$. The gauge-invariant tunneling for the ground state qubit is created via two far-detuned dipole-allowed Raman transitions of detunings Δ and $\Delta+\delta$, depicted by black arrows, that virtually couple the qubit states in the $S_{1/2}$ level to an excited state in the $P_{3/2}$ level. Fpr the optical qubit, these far-detuned Raman transitions are quadrupole-allowed, and virtually couple the $S_{1/2}$ level to a metastable state in the $D_{5/2}$ level. When the beat note of the two tones δ is on resonance with the difference of two secular trap frequencies, we attain the desired state-dependent parametric tunneling.

Raman transition [227]. The two beams are assumed to be counter-propagating $\boldsymbol{k}_{\rm L,1} = -\boldsymbol{k}_{\rm L,2} =: \boldsymbol{k}$, such that the beat note wave-vector is $\boldsymbol{k}_{\rm d} = 2\boldsymbol{k}$. Moreover, we assume that the angle between $\boldsymbol{k}_{\rm d}$ and the axial mode (z) is 45°, while the angle with respect to the transverse mode (x) is 60°.The two Raman beams at near $\lambda = 402\,$nm are detuned by $\Delta/2\pi = 10\,$THz from the $S_{1/2} \leftrightarrow P_{3/2}$ transition (see Supplementary Figure 3). The Lamb-Dicke factors (81) of the two motional modes are $\eta_z = 2\times 0.077$ and $\eta_x = 2\times 0.043$. In this system, light shifts of up to $\Omega_{1,2}/2\pi = 1.1\,$MHz can be achieved. In the full Hamiltonian (16), we set the beam detunings to $\delta = \omega_x - \omega_z$, resulting in a beat note frequency of $\omega_{\rm d} = \delta$ in Eq. (82). These parameters lead to an estimated coupling of $\Omega_{1,2}/2\pi = 1.1\,$MHz, which sets the timescale of the targeted dynamics shown in 7 of the main text.

In this figure, there is a clear agreement with small deviations from the expected dynamics of the $\mathbb{Z}_2$ gauge link. To quantify these deviations in more detail, we numerically solve the trapped-ion evolution, starting in $|\mathrm{L}\rangle$ (9), where we apply the interaction for a duration $t = \Delta t_{\rm ex}$ such that, by the end of it, the overlap squared to the desired state $|\mathrm{R}\rangle$ is maximised. If we consider only the idealised tunneling term, Eq. (21), the exchange duration would be given by $\Delta t_{\rm ex} = \pi/2t_{1,\mathbf{e}_1}$. In the simulation of the more realistic trapped-ion case, there are additional terms neglected in the ideal case that can change the optimal exchange duration. We thus find $\Delta t_{\rm ex}$ by maximising the fidelity $\mathscr{F}(t) = |\langle \mathrm{R}|\psi(t)\rangle|^2$ of achieving the desired state $|\mathrm{R}\rangle$. We also calculate the expectation value of the local symmetry generators (7) for $\langle G_1(t) + G_2(t)\rangle/2$ to check if the effective gauge symmetry is fulfilled. Moreover, when introducing the electric field with magnitude h in the simulations, we plot the maximum contrast $\mathscr{C}$ in the oscillations of

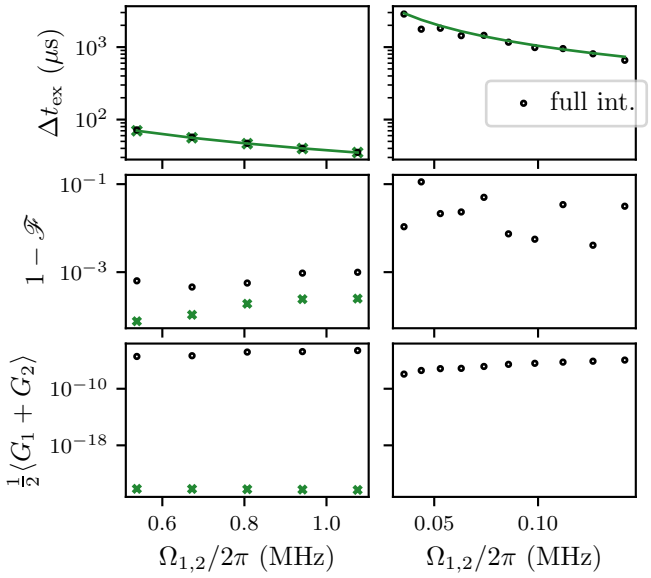

Supplementary Figure 4. **Light-shift $\mathbb{Z}_2$ tunneling with Raman couplings:** Numerical simulations of the exchange duration Δt_{ex} (upper panel), state infidelity $1-\mathscr{F}$ (middle panel), and Gauss' symmetry operator $\langle G_1+G_2\rangle/2$ as a function of the two-photon light shift $\Omega_{1,2}$ for dipole-allowed couplings (left column) and quadrupole-allowed couplings (right column). The results are shown for the full Hamiltonian (16) (black) and the idealized invariant-gauge tunneling (21) (green). The green solid line in the upper panel is the analytic dependence of the exchange duration on $\Omega_{1,2}$, extracted from Eq. (23). For both the full and ideal Hamiltonian the expectation value of the symmetry operator is consistent with 0, down to 10^{-3}.

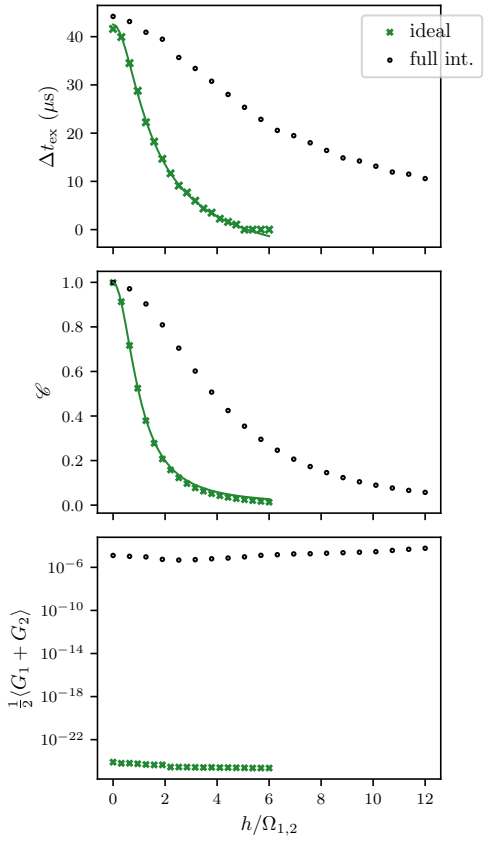

Supplementary Figure 5. **Light-shift $\mathbb{Z}_2$ tunneling with a non-zero electric field:** we simulate the hopping duration, contrast $\mathscr{C}$ and symmetry operator $\langle G_1+G_2\rangle/2$ as a function of electric field strength h relative to the two-photon light shift $\Omega_{1,2}$ of the dipole-allowed transitions. The results are shown for the full Hamiltonian (16) (black), including the additional carrier driving (3) with a modified resonant condition (28). We also show the results for the ideal gauge-invariant Hamiltonian (29) (green). The green solid line is the analytic dependence of the exchange duration and contrast respectively on $\Omega_{1,2}$, extracted from Eqs. (10) and the effective couplings (23) and (30). For both the full and ideal cases , the expectation value of the symmetry operator is consistent with 0, down to 10^{-3}.

$\bar{s}_x(t)$ (11). Thus, we can evaluate the reduced tunneling probability caused by the energy penalty for stretching/compressing the electric field line as one increases $h>0$.

In Supplementary Figure 4, we present simulations of the resulting hopping duration Δt_{ex}, the fidelity error $1-\mathscr{F}(t)$ and the gauge-invariance operator $\langle G_1(t)+G_2(t)\rangle/2$ as a function of applied light shift $\Omega_{1,2}$, which can be increased by using higher laser intensities or lower Raman detunings in order to obtain a faster gauge-invariant dynamics (23). When comparing the dynamics of the full Hamiltonian to the ideal gauge-invariant tunneling (23), we observe excellent agreement with $\Delta t_{ex}=\pi/2t_{1,\mathbf{e}_1}$. The fidelity error and the symmetry operator $\langle G_1(\Delta t_{ex})+G_2(\Delta t_{ex})\rangle/2$ also remain very low even when including the trapped-ion additional terms such as the off-resonant carrier, which underlies the adequacy of the considered parameters for this specific scheme. We can achieve an effective tunneling rate of up to 7.1 kHz inferred as $1/(4\Delta t_{ex})$.

To achieve large tunneling rates given the achievable $\Omega_{1,2}$ of current systems, and the low coupling rate of the second-order process $\propto\eta_x\eta_z$ (23), one needs to push the parameters to a regime that violates the $\delta\gg|\Omega_{1,2}|$ requirement. This results in off-resonant driving of spurious interactions, most prominently direct off-resonant carrier coupling. As mentioned above we minimise this effect by employing adiabatic amplitude pulse shaping [317] with a rise time of 10 µs.

We now present similar simulations for the light-shift type scheme as a function of the effective electric-field strength h. In Supplementary Figure 5, we present the exchange duration Δt_{ex} defined at maximum state fidelity $\mathscr{F}$, the maximum contrast $\mathscr{C}$ in $\bar{s}_x(t)$, and the expectation value of the gauge-symmetry generators $\langle G_1+G_2\rangle/2$, all of them as a function of the ratio between the transverse electric field h and the differential ac-Stark shift amplitude $\Omega_{1,2}$. While the presence of the non-commuting carrier coupling (z basis) present in the full Hamiltonian reduces the effect of the transverse term (x basis) from that of the ideal case, the gauge invariance is preserved.

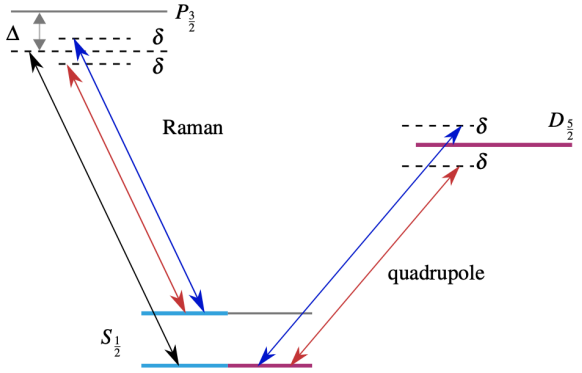

Supplementary Figure 6. **Mølmer-Sørensen-type parametric drive:**. For the ground state qubit (cyan lines), the Raman scheme which is now near resonant with the qubit frequency $\omega_0 + \delta$, we need to introduce a third tone, here depicted by a blue arrow . For the optical qubit (magenta lines), which is driven directly via the quadrupole transition, we symmetrically detune the two tones (blue and red) about the qubit resonance by $\pm\delta$.

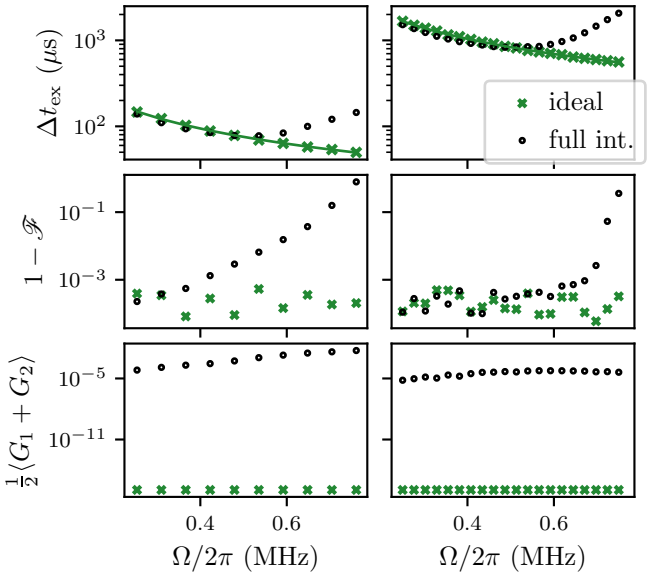

Supplementary Figure 7. **Mølmer-Sørensen-type $\mathbb{Z}_2$ tunneling:** Simulation of the exchange duration, fidelity error, and symmetry operator $\langle G_1 + G_2\rangle/2$ as a function of the two-photon Rabi frequency Ω for dipole-allowed Raman transitions (left column) and the single-photon Rabi frequency Ω for quadrupole-allowed transitions (right column). The results are shown for the full Hamiltonian (24) (black) and the idealized invariant-gauge tunneling (25) (green). The green solid line in the upper panel is the analytic dependence of the exchange duration on Ω, extracted from Eq. (26). For both the full and ideal Hamiltonian the expectation value of the symmetry operator is consistent with 0, as desired, down to 10^{-3}.

Quadrupole light-shift scheme

In this Appendix, we discuss the implementation of the analog scheme based on optical qubits. For a $^{88}Sr^+$ ion with the same parameters as in the previous Appendix, the optical qubit is formed by the ground state $5S_{1/2}, m_j = -1/2$ and the metastable state $4D_{5/2}, m_j = -1/2$ (see Supplementary Figure 3). To estimate realistic numbers for the light-shift scheme on the optical qubit, we consider a narrow-linewidth 674 nm laser system [229]. The Lamb-Dicke factor changes due to the different wavelength of the two laser beams, leading to $\eta_z = 2 \times 0.05$ and $\eta_x = 2 \times 0.024$. We employ two 674-nm beams detuned with respect to the qubit resonance by $\delta = \omega_x - \omega_z$, where $\Delta = 2\pi \cdot 3.56\,\text{MHz}$. The detuning Δ is much smaller than for the dipole-allowed Raman transitions on the left of Supplementary Figure 3, as the $D_{5/2}$ level is metastable and its lifetime is much longer than the timescale of interest. In Supplementary Figure 7, we present the results of our numerical simulations for the same quantities as above, but as a function of the Rabi-frequency Ω for the optical qubit. In this case, we can achieve tunneling coupling rates of up to 0.17 kHz inferred as $1/(4\Delta t_{\rm ex})$, which are much slower than the dipole-Raman scheme. Likewise, the state infidelity is larger, showing that the realization with optical qubits will be more challenging.

Mølmer-Sørensen-type scheme

A challenge with this scheme when applied to the quadrupole transition is the large resulting light shift $\Delta E_{\rm ac}$ on the qubit transition. This spurious term is $1/(\eta_x\eta_z)$ larger than the sought-after tunneling rate. This issue can be circumvented by either combining the tunneling interaction with a spin-echo [227] or by tracking the qubit frequency shift in software and feed-forward the acquired phase. The first approach is no longer compatible when a transverse electric-field term is added (see Eq. (5)). The second approach is in principle possible, but relies on the precise calibration of the Stark shift, as the beams used to generate the transverse electric-field term must be tuned accordingly (see Eq. (28)). This is a challenging task, as the shift needs to be calibrated to a precision that goes well beyond that of the effective tunneling rate. Moreover, pulse shaping makes the calibration more difficult, as the instantaneous light shift changes over the pulse duration. In practice, this is difficult as the light-shift amplitude is $1/\eta_x\eta_z$ larger than the tunneling interaction, and would need to be calibrated to a precision exceeding the tunneling rate. Hence, no simulations are included for the light-shift scheme utilising the quadrupole coupling.

In this Appendix, we present a detailed analysis of possible errors in the MS parametric tunneling, considering realistic trapped-ion parameters for both the ground state and optical qubit schemes of Supplementary Figure 6. Once again, we numerically integrate the full dynamics for (24) and compare it to the idealized tunneling term (25). For the Raman scheme for the ground state qubit, the bichromatic field can be achieved by having one Raman beams at $\omega_L + \omega_0$ and the other counter-propagating Raman beam consisting of two tones at $\omega_L \pm \delta$, i.e. $\boldsymbol{k}_{\rm d} = 2\boldsymbol{k}$. For the optical qubit, on the other

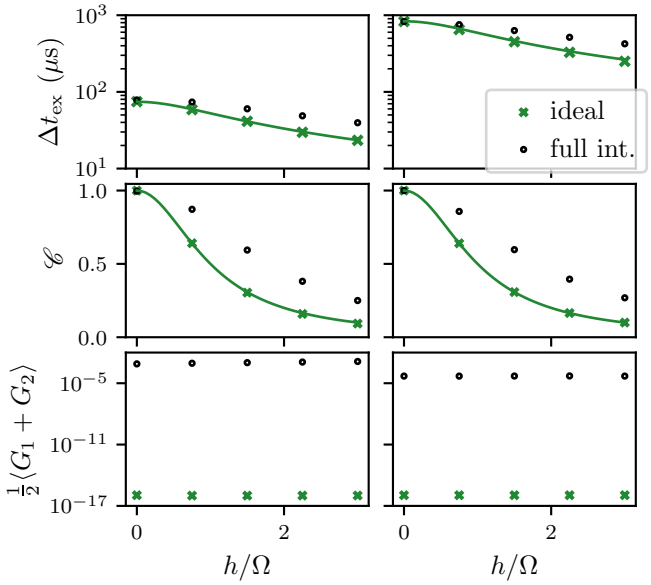

Supplementary Figure 8. **Mølmer-Sørensen $\mathbb{Z}_2$ tunneling with a non-zero electric field:** with Raman couplings (left column) and quadrupole couplings (right column). Simulating the exchange duration, contrast, and symmetry operator $\langle G_1+G_2\rangle/2$ as a function of electric field strength h relative to the coupling strength Ω. The results are shown for the full Hamiltonian (24) (black), including the additional carrier driven by a simple shift of the Mølmer-Sørensen detuning (32). We also show the results for the ideal gauge-invariant Hamiltonian (31) (green). The green solid line in the upper panel is the expected analytic dependence of the exchange duration on Ω, extracted from Eqs. (10) and the effective couplings (26) and (32). For both the full and ideal Hamiltonian the expectation value of the symmetry operator is consistent with 0, as desired, down to 10^{-3}.

hand, one can obtain a similar coupling by addressing it with a single beam consisting of two tones at $\omega_0 \pm \delta$, i.e. $\boldsymbol{k}_d = \boldsymbol{k}$. The Rabi frequency Ω of the blue- $(+\delta)$ and red-detuned $(-\delta)$ tone must be the same. We assume the same experimental parameters as in the previous section. For implementing this on the optical qubit we use the quadrupole transition at $\lambda = 674$ nm. The Lamb-Dicke parameters are $\eta_z = 0.05$ and $\eta_x = 0.024$, and we consider Rabi frequencies of up to $\Omega/2\pi = 1.1\,\mathrm{MHz}$. As previously, we truncate the phonon occupations to $n_{\max} = 7$ phonons. We obtain a maximum effective tunneling coupling strength $3.22\,\mathrm{kHz} = 1/(4\Delta t_{ex})$ for the Raman scheme, and a slower one $0.30\,\mathrm{kHz} = 1/(4\Delta t_{ex})$ for the quadrupole scheme (see Supplementary Figure 7).

We note that a similar principle has been recently used to generate single-mode squeezing in reference [318], which can then be used for the quantum simulation of spin models with multi-spin interactions [214, 215, 319]. We add adiabatic pulse shaping to the simulation as it enables smooth transitioning into the interaction picture and suppresses off-resonant (non-commuting) carrier excitations. This effectively reduces the strength of the tunneling but, importantly, it retains the state dependence. The non-commuting carrier sets a limit on the achievable interaction magnitude;, which is reflected by the global minimum in the duration (first row, Supplementary Figure 7).

Let us now present the error analysis for the MS scheme when considering an additional electric-field term as discussed around Eq. of the main text. The resulting exchange duration Δt_{ex}, the maximum contrast $\mathscr{C}$ in $\bar{s}_x(t)$ and gauge-symmetry generators $\langle G_1+G_2\rangle/2$, found through numerical simulations of the Hamiltonian (31) and are compared to the ideal gauge tunneling (5) (see Supplementary Figure 8). As before, the presence of the off-resonant carrier reduces the effective magnitude of the transverse term, but gauge invariance is preserved.

Orthogonal-force pulsed scheme

In this appendix, we consider the same experimental apparatus as in previous ones, and investigate the implementation of the gauge-invariant tunneling using the two orthogonal state-dependent forces.One way to implement the two orthogonal state-dependent forces in a laser system is by having two sets of Mølmer-Sørensen-style bichromatic fields. One bichromatic field is symmetrically detuned from the carrier by $\delta_1 = \pm(\omega_z + \delta)$ and the other by $\delta_2 = \pm(\omega_x + \delta)$. The bichromatic fields can either couple levels in the ground state via a Raman transition, or two levels of an optical qubit via a quadrupole transition. Moreover, for having two orthogonal state-dependent forces, we set the phase between the two bichromatic beams such that

$$\left(\frac{\phi_+ + \phi_-}{2}\right)_2 = \left(\frac{\phi_+ + \phi_-}{2}\right)_1 + \frac{\pi}{2}, \tag{90}$$

where ϕ_+, ϕ_- are the phases of the blue and red detuned tones in each of the bichromatic fields, 1 and 2. Applying these four tones gives rise to the two orthogonal state-dependent forces (34) that are needed for engineering the tunneling term (35). We consider the optical qubit and two motional modes with $\eta_z = 0.05$, $\omega_z/2\pi = 1.2$ MHz, and $\eta_x = 0.024$, $\omega_x/2\pi = 1.9\,\mathrm{MHz}$, respectively. We choose the detuning of the bichromatic fields from the respective vibrational mode to be $\delta/2\pi = 75\,\mathrm{kHz}$, and set $\Omega/2\pi = 0.75/\sqrt{2}$ MHz for each of the four tones. This should allow us to reach an effective tunneling coupling rate of up to 1.3 kHz, inferred as $1/(4\Delta t_{ex})$.

Let us note that the bichromatic scheme also leads to spurious carrier terms that drive off-resonant qubit rotations around axes that are orthogonal to each of the corresponding state-dependent forces. As mentioned above, a technique to mitigate the effect of the carrier term is pulse shaping [317], which is mainly needed at large coupling strengths, i.e., large Ω in Eq. (34). We describe the amplitude shaping of the pulses and further discuss its effect in our numerical simulations below.

The shortest time step that we can use in order to close the loops in phase space is $2\pi/\delta$, which was used for the simulations above. Hence, the Trotter error is given as $ht_{1,e_1}(2\pi/\delta)^2$ which must be negligible. In the simulation results presented above, for the highest value of h, the Trotter error was $\approx 8\times10^{-4}$. Higher values of δ reduce the $O([\eta\Omega/\delta]^3)$ error, and enable finer time steps in the time scans, as we always

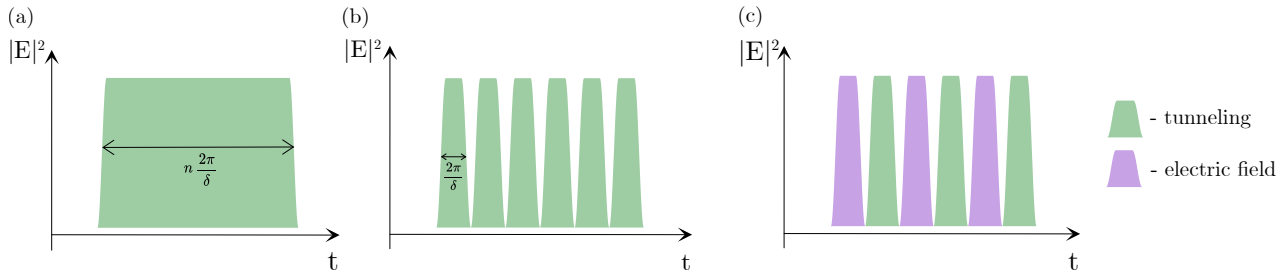

Supplementary Figure 9. **Amplitude-shaped pulses for the pulsed scheme:** (a) Shaped pulse that could be used for implementing just the tunneling term. (b) Trotterized pulse sequence for implementing the tunneling term. (c) Trotterized pulse sequence for implementing the full $\mathbb{Z}_2$-link Hamiltonian.

want to measure at instants where the loops in phase space that arise from first-order contributions in the Magnus expansion are closed, and the leading effect is the state-dependent tunneling. However, a higher δ also reduces the effective tunneling rate (35). This translates into shorter pulses which, when becoming comparable to the ramp length, do not give the effective desired dynamics anymore. Comparing the analog and pulsed schemes in terms of observing the matter-gauge field dynamics, the state preparation and measurement stages are the same. The difference is how the effective Hamiltonian in Eq. (5) is experimentally implemented and that is by using a pulse sequence as the one shown in Supplementary Figure 9 **(c)**. This was simulated as a series of pulses that are ramped on and off with $3.6\,\mu$s ramp durations and with the FWHM duration of $2\pi/\delta$, as shown in Fig Supplementary Figure 9 **(b)**. The same dynamics can be achieved by having a single pulse with the FWHM duration equal to an integer multiple of $2\pi/\delta$ (see Fig Supplementary Figure 9 **(a)**). By inspecting the figure more closely, we see that there are small deviations with respect to the idealized Hamiltonian (35) that deserve a more detailed analysis.

In the top panel of Supplementary Figure 10, we vary Ω in each one of the tones and evaluate how this affects the exchange duration $\Delta t_{\rm ex}$, calculated by maximising the state fidelity as in the previous section. We conduct simulations for three cases. Initially, we simulate the interaction in Eq. (34) that only contains the two orthogonal state-dependent forces. We then introduce the off-resonant carrier terms, which would arise from the Lamb-Dicke expansion of Eq. (24) as the leading off-resonant perturbations to the state-dependent forces (34). Finally, we also consider the amplitude pulse shaping. When the carrier terms are excluded, and the pulse is applied for a duration that is an integer multiple of $2\pi/\delta$, the inferred tunneling duration follows closely the theory from Eq. (35), which is represented by a green solid line according to $\Delta t_{\rm ex} = \pi/2t_{1,\mathbf{e}_1}$ with the effective tunneling of Eq. (36). As Ω is increased, the error term $O([\eta\Omega/\delta]^3)$ becomes significant, and small deviations start to appear. As above, we use the state fidelity $\mathscr{F}$ (the overlap to the desired state) and $\langle G_1+G_2\rangle/2$ (the expectation value of the symmetry generators) in order to evaluate the quality of the effective Hamiltonian with respect to Eq. (5). Introducing the carrier terms does not change the exchange duration $\Delta t_{\rm ex}$, $\mathscr{F}$, or $\langle G_1+G_2\rangle/2$ significantly. However, amplitude shaping the pulses substantially improves the quality of tunneling as it suppresses the coupling to higher order terms $O([\eta\Omega/\delta]^3)$. Introducing the amplitude-shaping ramp effectively decreases the area of the pulses, which translates into slightly slower exchange durations (top panel), but also leads to smaller errors (middle and bottom panels).

Once the viability of trapped-ion pulsed Scheme for the quantum simulation of the $\mathbb{Z}_2$ gauge-invariant tunneling has been demonstrated, we can consider the errors that would stem from adding the electric field term. In Fig Supplementary Figure 11, we present our numerical results, evaluating the decrease in contrast of the Rabi oscillations between the $|\mathrm{L}\rangle$ and $|\mathrm{R}\rangle$, and $\langle G_1+G_2\rangle/2$, as one increases the electric field h. When the carrier terms are excluded and we do not use the amplitude-shaped pulses, the decrease, in contrast, follows Eq. (11), which is represented as a green solid line in the top panel. We find that, in the realistic experimental situation with carrier terms present, and using amplitude-shaped pulses, we need slightly higher values of h to achieve the same contrast. This is mainly due to the effect of the ramp.

Supplementary Note 3: Wannier-Stark solution and MPS benchmark

In this Appendix, we discuss in detail the numerical benchmarks of MPS methods using exact solutions for the confinement dynamics in the one- (63) and two-boson (67) sectors.

One-boson sector

Considering that the tunneling strength is homogeneous $t_{i,\mathbf{e}_1} = \Omega_{\rm d}/4$, $\forall i$, and that the initial state contains a single boson (63), the effective Wannier-Stark ladder can be solved exactly in the thermodynamic limit $N\to\infty$. Shifting the zero energy to the center of the chain, the problem can be mapped onto the dynamics of a single planar rotor [267]. Let us discuss some of the details. A particle in a circle can be described in the basis $\{|\varphi\rangle\}$ determined by its angle $\varphi\in[0,2\pi)$. In this

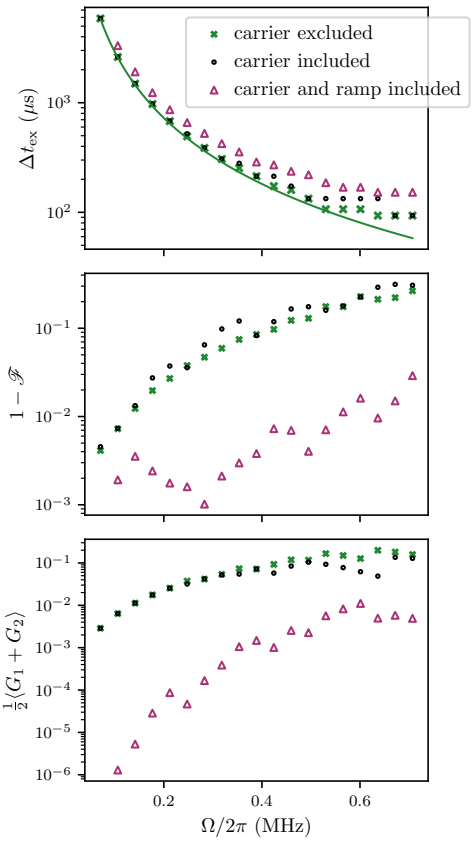

Supplementary Figure 10. **Pulsed-scheme $\mathbb{Z}_2$ tunneling with orthogonal forces:** We vary the strength of the tones in the bichromatic field Ω, and evaluate the exchange duration, the infidelity in obtaining the desired state $|R\rangle$, and the expectation value of the local symmetry generators. We do this for three cases: excluding the carrier from the interaction and thus considering Eq. (34) (green crosses); looking at the full interaction and thus including the spurious carrier terms (black circles); and, finally, considering the full interaction while slowly ramping the pulses on and off (magenta triangles). The green solid line in the upper panel is the expected analytic dependence of the exchange duration on Ω, extracted from Eq. (36). For the Hamiltonian including the spurious carrier and adiabatic ramp the expectation value of the symmetry operator is consistent with 0, as desired, down to 10^{-2}.

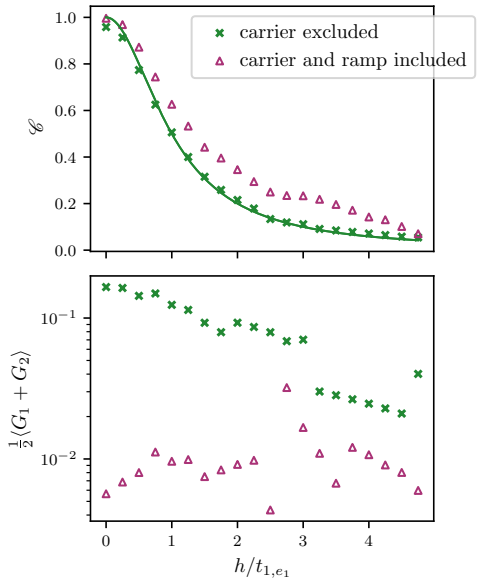

Supplementary Figure 11. **Pulsed-scheme $\mathbb{Z}_2$ tunneling with orthogonal forces in the presence of a non-zero electric field**: We simulate the $\mathbb{Z}_2$ dynamics using two orthogonal spin-dependent forces for different magnitudes of h. The value used for t_{1,e_1} was calculated as $1/(4\Delta t_{\rm ex})$ at $h=0$. We obtain dynamics similar to 3 **(b)** and infer the maximum contrast in $\bar{s}_x(t)$ and the expectation value of the local symmetry at the point of maximum contrast. The markers are numerical simulations, while the continuous lines are analytical predictions for different values of h Eq. (11). For the Hamiltonian including the spurious carrier and adiabatic ramp the expectation value of the symmetry operator is consistent with 0, as desired, down to 10^{-2}.

basis, the angular momentum $J_z=-\mathrm{i}\partial_\varphi$ is a Hermitian operator, and it readily follows that its spectrum is a countable infinite set $\sigma(J_z)=\mathbb{Z}$. Moreover, one can introduce the unitary ladder operators $J_\pm=\mathrm{e}^{\pm\mathrm{i}\varphi}$, and find a representation of the $O(2)$ rotor algebra $[J_z,J_\pm]=\pm J_\pm$, and $[J_+,J_-]=0$, which differs from the more standard $SU(2)$ algebra of spin operators. Using the physical states (62) of the $\mathbb{Z}_2$ gauge theory in the thermodynamic limit, one can readily find a specific representation of the rotor algebra

$$J_z=\sum_{i\in\mathbb{Z}} i\,|{\sim}\bullet_i\rangle\langle{\sim}\bullet_i|\,,\quad J_\pm=\sum_{i\in\mathbb{Z}}|{\sim}\bullet_{i\pm1}\rangle\langle{\sim}\bullet_i|\,,\qquad(91)$$

where we see that the position of the $\mathbb{Z}_2$ charge with the attached electric-field line maps onto the angular momentum of the rotor, whereas the tunneling to the right (left) map onto the rotor ladder operators $J_+(J_-)$.

It is then straightforward to derive the Heisenberg equations for the mean position and standard deviation of the $\mathbb{Z}_2$ charged boson. For instance, considering that the boson is initially in the middle of the chain $|\Psi_{\rm phys}(0)\rangle=|{\sim}\bullet_{N/2}\rangle$, we find that the mean is $\langle J_z(t)\rangle=N/2$, while the standard deviation oscillates

$$\sigma(t)=(\langle J_z^2(t)\rangle-\langle J_z(t)\rangle^2)^{1/2}=(\sqrt{2}t_{i,\mathbf{e}_1}/h)\sin(ht).\qquad(92)$$

We thus see that the average position of the boson attached to the electric-field line remains constant. However, this is not the signature of the aforementioned Wannier-Stark localisation yet. Indeed, setting $h=0$ yields the same result, as an initially localised particle in a tight-binding model with the same amplitude of tunneling to the left and right can only disperse around the initial position, but its average position remains static. In this limit, the above expression of the standard deviation leads to a ballistic dispersion $\sigma(t)=(\sqrt{2}t_{1,\mathbf{e}_1})t$, which differs clearly from the breathing-type oscillations that appear as soon as $h\neq0$. Hence, it is the change in the dispersion which provides a signature of the Wannier-Stark localisation of the $\mathbb{Z}_2$ charge, which can only disperse within

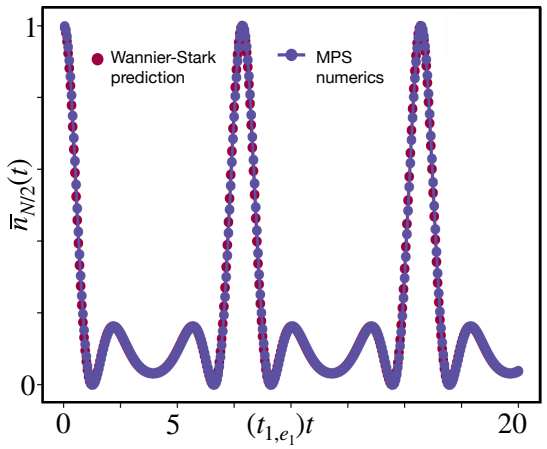

Supplementary Figure 12. **Wannier-Stark localisation of a single boson:** We compare the analytical prediction for $\overline{n}_{N/2}(t) = \langle a^\dagger_{N/2} a_{N/2}(t)\rangle$ in Eq. (95) to the numerical results based on Matrix Product states with bond dimension $\chi = 100$ for a chain with $N = 16$ lattice sites. We set the transverse electric field to $h = 0.4t_{1,\mathbf{e}_1}$ and we use the time step $\delta t = 0.05/t_{1,\mathbf{e}_1}$. The analytical formula (95) is based on the mapping of the $\mathbb{Z}_2$ gauge theory for a single boson (63) to the Wannier-Stark ladder in the thermodynamic limit of an infinitely-long chain.

a localised region by periodically stretching and compressing the attached electric-field string.

To provide a more complete description of this localisation, we note that the thermodynamic problem has an exact solution in terms of the so-called Wannier-Stark eigenstates

$$|\varepsilon_m\rangle = \sum_{i\in\mathbb{Z}} (-1)^{i-m} J_{i-m}(\gamma)\,|{\sim}\bullet_i\rangle\,, \quad \gamma = \frac{t_{i,\mathbf{e}_1}}{h} \tag{93}$$

where $J_n(x)$ is the first-class Bessel function of integer order n, and the corresponding energies $\varepsilon_m = m(2h)$ define the aforementioned Wannier-Stark ladder for $m \in \mathbb{Z}$. This solution can be derived by going to momentum space and using the Hansen-Bessel integral representation [266, 267] or, more directly, by looking into the discrete difference equation for the amplitudes of the eigenstates in the physical basis

$$|\varepsilon_m\rangle = \sum_{i\in\mathbb{Z}} c_i\,|{\sim}\bullet_i\rangle\,, \quad t_{i-1,\mathbf{e}_1} c_{i-1} + t^*_{i,\mathbf{e}_1} c_{i+1} + 2hi\,c_i = \varepsilon_m c_i\,. \tag{94}$$

This equation can be rewritten in terms of the recurrence relation of Bessel functions [320], such that one can identify $c_i = (-1)^{i-m} J_{i-m}(\gamma)$, and check for the consistency of normalisation $\sum_{i\in\mathbb{Z}} |c_i|^2 = \sum_{i\in\mathbb{Z}} J^2_{i-m}(\gamma) = 1$. In light of the asymptotic scaling of the Bessel functions, which vanish rapidly for $|i-m| \gg \gamma$, one can see that the eigenstates (93) are not delocalised over the whole lattice as occurs for $h \to 0$ but, instead, concentrated around the m-th site, which is a more direct manifestation of the so-called Wannier-Stark localisation that parallels the definition of Anderson localisation in disordered systems [321].

With these eigenstates, one can construct the full unitary propagator of the problem. Using the Neumann-Graff addition formula of Bessel functions [322], the probability to find the boson with the attached electric-field line r sites apart is $p_r(t) = |\langle {\sim}\bullet_{N/2+r}|\Psi_{\rm phys}(t)\rangle|^2 = J^2_r\big(2\gamma\sin(ht)\big) = p_{-r}(t)$. In comparison to the Rabi oscillations of the single-link case in Fig. 3 (main text), where the boson and the gauge field oscillate in phase according to the observables of Eq. (11), we now have correlated Wannier-Stark oscillations in both the number of bosons

$$\overline{n}_i(t) = \langle a^\dagger_i a_i(t)\rangle = p_i(t) = J^2_{i-N/2}\big(2\gamma\sin(ht)\big), \tag{95}$$

and the position of the electric-field line attached to the boson, which can be inferred from the two-point correlation function

$$\langle \sigma^x_{i-1,\mathbf{e}_1}\sigma^x_{i,\mathbf{e}_1}(t)\rangle = 1 - 2J^2_{i-N/2}\big(2\gamma\sin(ht)\big). \tag{96}$$

In Supplementary Figure 12 , we present a quantitative comparison of the analytical prediction for the boson number operator at the center of the chain $\overline{n}_{N/2}(t)$ in Eq. (95) with the numerical results based on MPS discussed in the main text. The agreement is remarkable, which serves to benchmark the validity of our approach.

Two-boson sector

In the two-boson sector, by introducing the center-of-mass $x_{\rm cm} = \frac{1}{2}(i+j)$, and relative coordinate $r = j - i \geq 0$, the problem (67) reduces to the Wannier-Stark ladder for a single particle in a one-dimensional chain. Noting once more that the tunneling strengths are homogeneous, one finds

$$c_{i,j} = \mathrm{e}^{\mathrm{i}Px_{\rm cm}} c(r), \quad t_P c(r-1) + t^*_P c(r+1) + 2hr\,c(r) = \varepsilon_{m,P} c(r), \tag{97}$$

where we have introduced the conserved total momentum $P = (p_i + p_j)$, the momentum-independent Wannier-Stark ladder energies $\varepsilon_{m,P} = m(2h)$, and the dressed tunneling strength

$$t_P = 2t_{1,\mathbf{e}_1}\cos(P/2)\,. \tag{98}$$

In contrast to Bose-Hubbard-type models with finite range interactions, which can lead to both scattering and bound states for a pair of bosons [279], the above recurrence equation (97) describes a relative particle that tries to tunnel against a linear potential with a dressed tunneling strength that depends on the center-of-mass momentum. Once again, by taking the thermodynamic limit, the recurrence equation corresponds to that of a Wannier-Stark ladder (94) for the relative particle. In this way, we obtain the following solutions

$$|\varepsilon_{m,P}\rangle = \sum_{i,j}{}' \sum_{m\in\mathbb{Z}} \mathrm{e}^{\mathrm{i}P(i+j)/2} (-1)^{j-i+m} J_{j-i-m}(\gamma_P)\,|_i{\bullet\!\!-\!\!\bullet}_j\rangle \tag{99}$$

where $\gamma_P = 2t_{1,\mathbf{e}_1}\cos(P/2)/h$. As occurred for the single-boson sector, where any of the m-th eigenstates (93) is localised around the m-th site, the two-particle solutions (99) only consist of bound states regarding their relative distance instead of scattering states. The original bosons are thus confined in pairs, forming wavefunctions of energy $\varepsilon_{m,P}$, which decay exponentially fast as their relative distance r increases

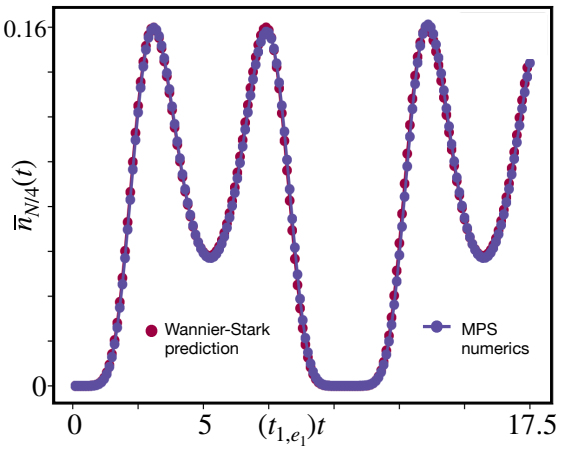

Supplementary Figure 13. **Wannier-Stark confinement for two bosons:** We compare the analytical prediction for $\bar{n}_{N/4}(t) = \langle a^\dagger_{N/4} a_{N/4}(t)\rangle$ in Eq. (100) to the numerical results based on Matrix Product states with bond dimension $\chi = 100$ for a chain with $N = 32$ sites. We set the transverse electric field to $h = 0.3t_{1,\mathbf{e}_1}$ and we use the time step $\delta t = 0.05/t_{1,\mathbf{e}_1}$. The analytical formula (100) is based on the mapping of the $\mathbb{Z}_2$ gauge theory for a boson pair (63) to the Wannier-Stark ladder for the particle of reduced mass in the thermodynamic limit of a chain.

$|r| > m$. These solutions are a toy analog of mesons in higher-dimensional non-Abelian gauge theories. The original particles, which carry a net $\mathbb{Z}_2$ charge, cannot be observed as individual excitations, just like quarks in quantum chromodynamics. They become instead confined in pairs of zero net charge, which are associated to a specific quantised bound energy depending on their respective confinement. In the present case, these meson-like particles can freely move as a whole, i.e. non-zero center-of-mass momentum.

Let us now consider an initial state in which the bosons are symmetrically positioned about the center of the chain with relative distance r_0, namely $|\Psi_{\text{phys}}(0)\rangle = |_{(N-r_0)/2}\bullet\!\sim\!\bullet_{(N+r_0)/2}\rangle$. This state has a vanishing total momentum $P = 0$, such that the center of mass will remain localised at the center of the chain while the two particles disperse and interfere. According to our previous discussion, the number of bosons (95) should now evolve according to

$$\bar{n}_i(t) = \left|J_{i-N/2-r_0/2}\big(2\gamma\sin(ht)\big) + J_{i-N/2+r_0/2}\big(2\gamma\sin(ht)\big)\right|^2. \tag{100}$$

In Supplementary Figure 13, we present a quantitative comparison of this analytical expression for $\bar{n}_{N/2}(t)$ with the TDVP numerical results. As found in the single-particle sector of Supplementary Figure 12, the agreement of the numerical TDVP results with the analytical prediction in terms of the sum of Bessel functions is remarkable, and serves to benchmark the validity of our approach, which will be extended to situations beyond analytical solutions below.

[1] P. W. Anderson, Science **177**, 393 (1972).
[2] L. Landau, Zh. Eksp. Teor. Fiz. **7**, 19 [Phys. Z. Sowjetunion 11, 26 (1937)] (1937).
[3] E. Fradkin, *Field Theories of Condensed Matter Physics*, 2nd ed. (Cambridge University Press, 2013).
[4] K. G. Wilson and J. Kogut, Physics Reports **12**, 75 (1974).
[5] T. J. Hollowood, *Renormalization Group and Fixed Points in Quantum Field Theory* (Springer, 2013).
[6] D. Gross, Proceedings of the National Academy of Sciences **93**, 14256 (1996).
[7] Y. Nambu, Phys. Rev. **117**, 648 (1960).
[8] J. Goldstone, A. Salam, and S. Weinberg, Phys. Rev. **127**, 965 (1962).
[9] C. N. Yang and R. L. Mills, Phys. Rev. **96**, 191 (1954).
[10] S. L. Glashow, Nuclear Physics **10**, 107 (1959).
[11] A. Salam and J. C. Ward, Il Nuovo Cimento (1955-1965) **11**, 568 (1959).
[12] S. Weinberg, Phys. Rev. Lett. **19**, 1264 (1967).
[13] G. Hooft, Nuclear Physics B **35**, 167 (1971).
[14] G. 't Hooft and M. Veltman, Nuclear Physics B **44**, 189 (1972).
[15] M. Gell-Mann, Phys. Rev. **125**, 1067 (1962).
[16] M. Gell-Mann, Physics Letters **8**, 214 (1964).
[17] H. Fritzsch, M. Gell-Mann, and H. Leutwyler, Phys. Lett. B **47**, 365 (1973).
[18] D. J. Gross and F. Wilczek, Phys. Rev. Lett. **30**, 1343 (1973).
[19] H. D. Politzer, Phys. Rev. Lett. **30**, 1346 (1973).
[20] P. W. Anderson, Phys. Rev. **130**, 439 (1963).
[21] P. W. Higgs, Phys. Rev. Lett. **13**, 508 (1964).
[22] M. E. Peskin and D. V. Schroeder, *An Introduction to quantum field theory* (Addison-Wesley, Reading, USA, 1995).
[23] J. Greensite, *Introduction to the confinement problem* (Springer Nature, 2020).
[24] J. B. Kogut and M. A. Stephanov, *The Phases of Quantum Chromodynamics: From Confinement to Extreme Environments*, Cambridge Monographs on Particle Physics, Nuclear Physics and Cosmology (Cambridge University Press, 2003).
[25] N. Brambilla *et al.*, Eur. Phys. J. C **74**, 2981 (2014), arXiv:1404.3723 [hep-ph].
[26] K. G. Wilson, Phys. Rev. D **10**, 2445 (1974).
[27] S. Durr, Z. Fodor, J. Frison, C. Hoelbling, R. Hoffmann, S. D. Katz, S. Krieg, T. Kurth, L. Lellouch, T. Lippert, K. K. Szabo, and G. Vulvert, "Ab-initio determination of light hadron masses," (2009), cite arxiv:0906.3599Comment: 22 pages, 3 Tables, 8 Figures. Published in Science (21 November 2008) with Supporting Online Material. Submission to arXiv has been delayed by 6 months to respect the journal's embargo policy.
[28] M. Troyer and U.-J. Wiese, Phys. Rev. Lett. **94**, 170201 (2005).
[29] K. Nagata, Progress in Particle and Nuclear Physics **127**, 103991 (2022).
[30] J. Schwinger, Phys. Rev. **128**, 2425 (1962).
[31] A. Casher, J. Kogut, and L. Susskind, Phys. Rev. Lett. **31**, 792 (1973).
[32] S. Coleman, R. Jackiw, and L. Susskind, Annals of Physics **93**, 267 (1975).
[33] G. 't Hooft, Nuclear Physics B **75**, 461 (1974).
[34] C. G. Callan, N. Coote, and D. J. Gross, Phys. Rev. D **13**,

1649 (1976).
[35] F. J. Wegner, Journal of Mathematical Physics **12**, 2259 (1971).
[36] X.-G. Wen, *Quantum field theory of many-body systems: from the origin of sound to an origin of light and electrons* (Oxford University Press, Oxford, 2007).
[37] X.-G. Wen, Rev. Mod. Phys. **89**, 041004 (2017).
[38] G. Baskaran and P. W. Anderson, Phys. Rev. B **37**, 580 (1988).
[39] N. Read and S. Sachdev, Phys. Rev. Lett. **66**, 1773 (1991).
[40] A. Kitaev, Annals of Physics **321**, 2 (2006), january Special Issue.
[41] J. Kogut and L. Susskind, Phys. Rev. D **11**, 395 (1975).
[42] R. Moessner, S. L. Sondhi, and E. Fradkin, Phys. Rev. B **65**, 024504 (2001).
[43] A. Kitaev, Annals of Physics **303**, 2 (2003).
[44] E. Dennis, A. Kitaev, A. Landahl, and J. Preskill, Journal of Mathematical Physics **43**, 4452 (2002).
[45] B. M. Terhal, Rev. Mod. Phys. **87**, 307 (2015).
[46] F. F. Assaad and T. Grover, Phys. Rev. X **6**, 041049 (2016).
[47] S. Gazit, M. Randeria, and A. Vishwanath, Nature Physics **13**, 484 (2017).
[48] S. Gazit, F. F. Assaad, S. Sachdev, A. Vishwanath, and C. Wang, Proceedings of the National Academy of Sciences **115**, E6987 (2018).
[49] A. Smith, J. Knolle, R. Moessner, and D. L. Kovrizhin, Phys. Rev. B **97**, 245137 (2018).
[50] S. Gazit, F. F. Assaad, and S. Sachdev, Phys. Rev. X **10**, 041057 (2020).
[51] E. J. König, P. Coleman, and A. M. Tsvelik, Phys. Rev. B **102**, 155143 (2020).
[52] P. Emonts, M. C. Bañuls, I. Cirac, and E. Zohar, Phys. Rev. D **102**, 074501 (2020).
[53] D. Robaina, M. C. Bañuls, and J. I. Cirac, Phys. Rev. Lett. **126**, 050401 (2021).
[54] U. Borla, B. Jeevanesan, F. Pollmann, and S. Moroz, Phys. Rev. B **105**, 075132 (2022).
[55] D. Horn, M. Weinstein, and S. Yankielowicz, Phys. Rev. D **19**, 3715 (1979).
[56] E. Ercolessi, P. Facchi, G. Magnifico, S. Pascazio, and F. V. Pepe, Phys. Rev. D **98**, 074503 (2018).
[57] G. Magnifico, D. Vodola, E. Ercolessi, S. P. Kumar, M. Müller, and A. Bermudez, Phys. Rev. D **99**, 014503 (2019).
[58] G. Magnifico, D. Vodola, E. Ercolessi, S. P. Kumar, M. Müller, and A. Bermudez, Phys. Rev. B **100**, 115152 (2019).
[59] U. Borla, R. Verresen, F. Grusdt, and S. Moroz, Phys. Rev. Lett. **124**, 120503 (2020).
[60] M. c. v. Kebrič, L. Barbiero, C. Reinmoser, U. Schollwöck, and F. Grusdt, Phys. Rev. Lett. **127**, 167203 (2021).
[61] G. Magnifico, M. Dalmonte, P. Facchi, S. Pascazio, F. V. Pepe, and E. Ercolessi, Quantum **4**, 281 (2020).
[62] F. M. Surace and A. Lerose, New Journal of Physics **23**, 062001 (2021).
[63] A. S. Aramthottil, U. Bhattacharya, D. González-Cuadra, M. Lewenstein, L. Barbiero, and J. Zakrzewski, Phys. Rev. B **106**, L041101 (2022).
[64] A. Das, U. Borla, and S. Moroz, "Fractionalized holes in one-dimensional $\mathbb{Z}_2$ gauge theory coupled to fermion matter – deconfined dynamics and emergent integrability," (2021).
[65] J. del Pino and O. Zilberberg, "Dynamical gauge fields with bosonic codes," (2023), arXiv:2211.12119 [quant-ph].
[66] Z.-Y. Ge and F. Nori, "Confinement-induced enhancement of superconductivity in a spin-$\frac{1}{2}$ fermion chain coupled to a $\mathbb{Z}_2$ lattice gauge field," (2022).
[67] E. C. Domanti, P. Castorina, D. Zappalà, and L. Amico, "Coherence of confined matter in lattice gauge theories at the mesoscopic scale," (2023), arXiv:2304.12713 [cond-mat.quant-gas].
[68] T. Sugihara, arXiv preprint hep-lat/0509045 (2005).
[69] D. González-Cuadra, L. Tagliacozzo, M. Lewenstein, and A. Bermudez, Phys. Rev. X **10**, 041007 (2020).
[70] J. Nyhegn, C.-M. Chung, and M. Burrello, Phys. Rev. Research **3**, 013133 (2021).
[71] W. Brenig, Phys. Rev. B **105**, 245105 (2022).
[72] S. Pradhan, A. Maroncelli, and E. Ercolessi, "Discrete abelian lattice gauge theories on a ladder and their dualities with quantum clock models," (2022).
[73] A. Florio, A. Weichselbaum, S. Valgushev, and R. D. Pisarski, "Mass gaps of a $\mathbb{Z}_3$ gauge theory with three fermion flavors in 1 + 1 dimensions," (2023), arXiv:2310.18312 [hep-th].
[74] R. P. Feynman, Int. J. Theor. Phys. **21**, 467 (1982).
[75] J. I. Cirac and P. Zoller, Nature Physics **8**, 264 (2012).
[76] I. Bloch, J. Dalibard, and S. Nascimbène, Nature Physics **8**, 267 (2012).
[77] R. Blatt and C. F. Roos, Nature Physics **8**, 277 (2012).
[78] E. Altman, K. R. Brown, G. Carleo, L. D. Carr, E. Demler, C. Chin, B. DeMarco, S. E. Economou, M. A. Eriksson, K.-M. C. Fu, M. Greiner, K. R. Hazzard, R. G. Hulet, A. J. Kollár, B. L. Lev, M. D. Lukin, R. Ma, X. Mi, S. Misra, C. Monroe, K. Murch, Z. Nazario, K.-K. Ni, A. C. Potter, P. Roushan, M. Saffman, M. Schleier-Smith, I. Siddiqi, R. Simmonds, M. Singh, I. Spielman, K. Temme, D. S. Weiss, J. Vučković, V. Vuletić, J. Ye, and M. Zwierlein, PRX Quantum **2**, 017003 (2021).
[79] H. Weimer, M. Müller, I. Lesanovsky, P. Zoller, and H. P. Büchler, Nature Physics **6**, 382 (2010).
[80] L. Tagliacozzo, A. Celi, A. Zamora, and M. Lewenstein, Annals of Physics **330**, 160 (2013).
[81] L. Tagliacozzo, A. Celi, P. Orland, M. W. Mitchell, and M. Lewenstein, Nature Communications **4**, 2615 (2013).
[82] A. W. Glaetzle, M. Dalmonte, R. Nath, I. Rousochatzakis, R. Moessner, and P. Zoller, Phys. Rev. X **4**, 041037 (2014).
[83] H. P. Büchler, M. Hermele, S. D. Huber, M. P. A. Fisher, and P. Zoller, Phys. Rev. Lett. **95**, 040402 (2005).
[84] E. Zohar and B. Reznik, Phys. Rev. Lett. **107**, 275301 (2011).
[85] E. Zohar, J. I. Cirac, and B. Reznik, Phys. Rev. Lett. **109**, 125302 (2012).
[86] D. Banerjee, M. Dalmonte, M. Müller, E. Rico, P. Stebler, U.-J. Wiese, and P. Zoller, Phys. Rev. Lett. **109**, 175302 (2012).
[87] E. Zohar, J. I. Cirac, and B. Reznik, Phys. Rev. Lett. **110**, 055302 (2013).
[88] D. Banerjee, M. Bögli, M. Dalmonte, E. Rico, P. Stebler, U.-J. Wiese, and P. Zoller, Phys. Rev. Lett. **110**, 125303 (2013).
[89] E. Zohar, J. I. Cirac, and B. Reznik, Phys. Rev. Lett. **110**, 125304 (2013).
[90] U.-J. Wiese, Annalen der Physik **525**, 777 (2013).
[91] E. Zohar, J. I. Cirac, and B. Reznik, Reports on Progress in Physics **79**, 014401 (2015).
[92] M. Dalmonte and S. Montangero, Contemporary Physics **57**, 388 (2016).
[93] M. C. Bañuls, R. Blatt, J. Catani, A. Celi, J. I. Cirac, M. Dalmonte, L. Fallani, K. Jansen, M. Lewenstein, S. Montangero, C. A. Muschik, B. Reznik, E. Rico, L. Tagliacozzo, K. Van Acoleyen, F. Verstraete, U.-J. Wiese, M. Wingate, J. Zakrzewski, and P. Zoller, The European Physical Journal D **74**, 165 (2020).
[94] M. C. Bañuls and K. Cichy, Reports on Progress in Physics **83**, 024401 (2020).
[95] M. Aidelsburger, L. Barbiero, A. Bermudez, T. Chanda,

A. Dauphin, D. González-Cuadra, P. R. Grzybowski, S. Hands, F. Jendrzejewski, J. Jünemann, G. Juzeliūnas, V. Kasper, A. Piga, S.-J. Ran, M. Rizzi, G. Sierra, L. Tagliacozzo, E. Tirrito, T. V. Zache, J. Zakrzewski, E. Zohar, and M. Lewenstein, Philosophical Transactions of the Royal Society A: Mathematical, Physical and Engineering Sciences **380**, 20210064 (2022).

[96] N. Klco, A. Roggero, and M. J. Savage, Reports on Progress in Physics **85**, 064301 (2022).

[97] C. W. Bauer, Z. Davoudi, A. B. Balantekin, T. Bhattacharya, M. Carena, W. A. de Jong, P. Draper, A. El-Khadra, N. Gemelke, M. Hanada, D. Kharzeev, H. Lamm, Y.-Y. Li, J. Liu, M. Lukin, Y. Meurice, C. Monroe, B. Nachman, G. Pagano, J. Preskill, E. Rinaldi, A. Roggero, D. I. Santiago, M. J. Savage, I. Siddiqi, G. Siopsis, D. Van Zanten, N. Wiebe, Y. Yamauchi, K. Yeter-Aydeniz, and S. Zorzetti, "Quantum simulation for high energy physics," (2022).

[98] C. W. Bauer, Z. Davoudi, N. Klco, and M. J. Savage, Nature Rev. Phys. **5**, 420 (2023).

[99] J. C. Halimeh, M. Aidelsburger, F. Grusdt, P. Hauke, and B. Yang, "Cold-atom quantum simulators of gauge theories," (2023), arXiv:2310.12201 [cond-mat.quant-gas].

[100] D. Horn, Physics Letters B **100**, 149 (1981).

[101] P. Orland and D. Rohrlich, Nuclear Physics B **338**, 647 (1990).

[102] S. Chandrasekharan and U.-J. Wiese, Nuclear Physics B **492**, 455 (1997).

[103] D. Banerjee, F.-J. Jiang, P. Widmer, and U.-J. Wiese, Journal of Statistical Mechanics: Theory and Experiment **2013**, P12010 (2013).

[104] E. Rico, T. Pichler, M. Dalmonte, P. Zoller, and S. Montangero, Phys. Rev. Lett. **112**, 201601 (2014).

[105] S. Kühn, J. I. Cirac, and M.-C. Bañuls, Phys. Rev. A **90**, 042305 (2014).

[106] T. Pichler, M. Dalmonte, E. Rico, P. Zoller, and S. Montangero, Phys. Rev. X **6**, 011023 (2016).

[107] L. Cardarelli, S. Greschner, and L. Santos, Phys. Rev. Lett. **119**, 180402 (2017).

[108] Y.-P. Huang, D. Banerjee, and M. Heyl, Phys. Rev. Lett. **122**, 250401 (2019).

[109] P. Silvi, Y. Sauer, F. Tschirsich, and S. Montangero, Phys. Rev. D **100**, 074512 (2019).

[110] L. Cardarelli, S. Greschner, and L. Santos, Phys. Rev. Lett. **124**, 123601 (2020).

[111] D. Banerjee and A. Sen, Phys. Rev. Lett. **126**, 220601 (2021).

[112] T. Felser, P. Silvi, M. Collura, and S. Montangero, Phys. Rev. X **10**, 041040 (2020).

[113] A. Lerose, F. M. Surace, P. P. Mazza, G. Perfetto, M. Collura, and A. Gambassi, Phys. Rev. B **102**, 041118 (2020).

[114] I. Papaefstathiou, A. Smith, and J. Knolle, Phys. Rev. B **102**, 165132 (2020).

[115] G. Magnifico, T. Felser, P. Silvi, and S. Montangero, Nature Communications **12**, 3600 (2021).

[116] T. V. Zache, M. Van Damme, J. C. Halimeh, P. Hauke, and D. Banerjee, "Achieving the continuum limit of quantum link lattice gauge theories on quantum devices," (2021).

[117] J. C. Halimeh, M. Van Damme, T. V. Zache, D. Banerjee, and P. Hauke, "Achieving the quantum field theory limit in far-from-equilibrium quantum link models," (2021).

[118] T. Hashizume, J. C. Halimeh, P. Hauke, and D. Banerjee, SciPost Phys. **13**, 017 (2022).

[119] D. Banerjee, E. Huffman, and L. Rammelmüller, arXiv preprint arXiv:2201.07171 (2022).

[120] J. C. Halimeh, P. Hauke, J. Knolle, and F. Grusdt, "Temperature-induced disorder-free localization," (2022).

[121] E. A. Martinez, C. A. Muschik, P. Schindler, D. Nigg, A. Erhard, M. Heyl, P. Hauke, M. Dalmonte, T. Monz, P. Zoller, and R. Blatt, Nature **534**, 516 (2016).

[122] H.-N. Dai, B. Yang, A. Reingruber, H. Sun, X.-F. Xu, Y.-A. Chen, Z.-S. Yuan, and J.-W. Pan, Nature Physics **13**, 1195 (2017).

[123] N. Klco, E. F. Dumitrescu, A. J. McCaskey, T. D. Morris, R. C. Pooser, M. Sanz, E. Solano, P. Lougovski, and M. J. Savage, Phys. Rev. A **98**, 032331 (2018).

[124] C. Schweizer, F. Grusdt, M. Berngruber, L. Barbiero, E. Demler, N. Goldman, I. Bloch, and M. Aidelsburger, Nature Physics **15**, 1168 (2019).

[125] C. Kokail, C. Maier, R. van Bijnen, T. Brydges, M. K. Joshi, P. Jurcevic, C. A. Muschik, P. Silvi, R. Blatt, C. F. Roos, and P. Zoller, Nature **569**, 355 (2019).

[126] F. M. Surace, P. P. Mazza, G. Giudici, A. Lerose, A. Gambassi, and M. Dalmonte, Phys. Rev. X **10**, 021041 (2020).

[127] N. Klco, M. J. Savage, and J. R. Stryker, Phys. Rev. D **101**, 074512 (2020).

[128] A. Mil, T. V. Zache, A. Hegde, A. Xia, R. P. Bhatt, M. K. Oberthaler, P. Hauke, J. Berges, and F. Jendrzejewski, Science **367**, 1128 (2020).

[129] B. Yang, H. Sun, R. Ott, H.-Y. Wang, T. V. Zache, J. C. Halimeh, Z.-S. Yuan, P. Hauke, and J.-W. Pan, Nature **587**, 392 (2020).

[130] Z.-Y. Zhou, G.-X. Su, J. C. Halimeh, R. Ott, H. Sun, P. Hauke, B. Yang, Z.-S. Yuan, J. Berges, and J.-W. Pan, Science **377**, 311 (2022).

[131] Y. Y. Atas, J. Zhang, R. Lewis, A. Jahanpour, J. F. Haase, and C. A. Muschik, Nature Communications **12**, 6499 (2021).

[132] C. W. Bauer, B. Nachman, and M. Freytsis, Phys. Rev. Lett. **127**, 212001 (2021).

[133] N. H. Nguyen, M. C. Tran, Y. Zhu, A. M. Green, C. H. Alderete, Z. Davoudi, and N. M. Linke, PRX Quantum **3**, 020324 (2022).

[134] A. Ciavarella, N. Klco, and M. J. Savage, Phys. Rev. D **103**, 094501 (2021).

[135] S. A Rahman, R. Lewis, E. Mendicelli, and S. Powell, Phys. Rev. D **104**, 034501 (2021).

[136] A. N. Ciavarella and I. A. Chernyshev, Phys. Rev. D **105**, 074504 (2022).

[137] Z. Wang, Z.-Y. Ge, Z. Xiang, X. Song, R.-Z. Huang, P. Song, X.-Y. Guo, L. Su, K. Xu, D. Zheng, and H. Fan, Phys. Rev. Research **4**, L022060 (2022).

[138] Y. Y. Atas, J. F. Haase, J. Zhang, V. Wei, S. M. L. Pfaendler, R. Lewis, and C. A. Muschik, "Real-time evolution of su(3) hadrons on a quantum computer," (2022).

[139] R. C. Farrell, I. A. Chernyshev, S. J. M. Powell, N. A. Zemlevskiy, M. Illa, and M. J. Savage, "Preparations for quantum simulations of quantum chromodynamics in 1+1 dimensions: (i) axial gauge," (2022).

[140] R. C. Farrell, I. A. Chernyshev, S. J. M. Powell, N. A. Zemlevskiy, M. Illa, and M. J. Savage, "Preparations for quantum simulations of quantum chromodynamics in 1+1 dimensions: (ii) single-baryon β-decay in real time," (2022).

[141] A. Frölian, C. S. Chisholm, E. Neri, C. R. Cabrera, R. Ramos, A. Celi, and L. Tarruell, Nature **608**, 293 (2022).

[142] C. Charles, E. J. Gustafson, E. Hardt, F. Herren, N. Hogan, H. Lamm, S. Starecheski, R. S. V. de Water, and M. L. Wagman, "Simulating $\mathbb{Z}_2$ lattice gauge theory on a quantum computer," (2023), arXiv:2305.02361 [hep-lat].

[143] S. P. Jordan, K. S. M. Lee, and J. Preskill, Science **336**, 1130 (2012).

[144] S. P. Jordan, K. S. Lee, and J. Preskill, arXiv preprint

arXiv:1112.4833 (2011).
[145] S. P. Jordan, H. Krovi, K. S. M. Lee, and J. Preskill, Quantum **2**, 44 (2018).
[146] S. Flannigan, N. Pearson, G. H. Low, A. Buyskikh, I. Bloch, P. Zoller, M. Troyer, and A. J. Daley, Quantum Science and Technology **7**, 045025 (2022).
[147] O. Boada, A. Celi, J. I. Latorre, and M. Lewenstein, Phys. Rev. Lett. **108**, 133001 (2012).
[148] A. Celi, P. Massignan, J. Ruseckas, N. Goldman, I. B. Spielman, G. Juzeliūnas, and M. Lewenstein, Physical review letters **112**, 043001 (2014).
[149] T. Ozawa and H. M. Price, Nature Reviews Physics **1**, 349 (2019).
[150] M. Mancini, G. Pagano, G. Cappellini, L. Livi, M. Rider, J. Catani, C. Sias, P. Zoller, M. Inguscio, M. Dalmonte, and L. Fallani, Science **349**, 1510 (2015), https://www.science.org/doi/pdf/10.1126/science.aaa8736.
[151] B. K. Stuhl, H.-I. Lu, L. M. Aycock, D. Genkina, and I. B. Spielman, Science **349**, 1514 (2015).
[152] L. F. Livi, G. Cappellini, M. Diem, L. Franchi, C. Clivati, M. Frittelli, F. Levi, D. Calonico, J. Catani, M. Inguscio, and L. Fallani, Phys. Rev. Lett. **117**, 220401 (2016).
[153] J. H. Han, J. H. Kang, and Y. Shin, Phys. Rev. Lett. **122**, 065303 (2019).
[154] N. R. Bernier, L. D. Tóth, A. Koottandavida, M. A. Ioannou, D. Malz, A. Nunnenkamp, A. K. Feofanov, and T. J. Kippenberg, Nature Communications **8**, 604 (2017).
[155] F. A. An, E. J. Meier, and B. Gadway, Science Advances **3**, e1602685 (2017).
[156] K. Fang, J. Luo, A. Metelmann, M. H. Matheny, F. Marquardt, A. A. Clerk, and O. Painter, Nature Physics **13**, 465 (2017).
[157] O. Zilberberg, S. Huang, J. Guglielmon, M. Wang, K. P. Chen, Y. E. Kraus, and M. C. Rechtsman, Nature **553**, 59 (2018).
[158] E. Lustig, S. Weimann, Y. Plotnik, Y. Lumer, M. A. Bandres, A. Szameit, and M. Segev, Nature **567**, 356 (2019).
[159] A. Dutt, M. Minkov, Q. Lin, L. Yuan, D. A. B. Miller, and S. Fan, Nature Communications **10**, 3122 (2019).
[160] A. Dutt, Q. Lin, L. Yuan, M. Minkov, M. Xiao, and S. Fan, Science **367**, 59 (2020).
[161] T. Chalopin, T. Satoor, A. Evrard, V. Makhalov, J. Dalibard, R. Lopes, and S. Nascimbene, Nature Physics **16**, 1017 (2020).
[162] W. H. Louisell, A. Yariv, and A. E. Siegman, Phys. Rev. **124**, 1646 (1961).
[163] H. A. Haus and J. A. Mullen, Phys. Rev. **128**, 2407 (1962).
[164] J. P. Gordon, W. H. Louisell, and L. R. Walker, Phys. Rev. **129**, 481 (1963).
[165] B. R. Mollow and R. J. Glauber, Phys. Rev. **160**, 1076 (1967).
[166] C. M. Caves, Phys. Rev. D **26**, 1817 (1982).
[167] K. Fang, Z. Yu, and S. Fan, Phys. Rev. Lett. **108**, 153901 (2012).
[168] K. Fang, Z. Yu, and S. Fan, Phys. Rev. B **87**, 060301 (2013).
[169] Y. Aharonov and D. Bohm, Phys. Rev. **115**, 485 (1959).
[170] K. Fang, Z. Yu, and S. Fan, Nature Photonics **6**, 782 (2012).
[171] Y. Chen, C. Neill, P. Roushan, N. Leung, M. Fang, R. Barends, J. Kelly, B. Campbell, Z. Chen, B. Chiaro, A. Dunsworth, E. Jeffrey, A. Megrant, J. Mutus, P. O'Malley, C. Quintana, D. Sank, A. Vainsencher, J. Wenner, T. White, M. R. Geller, A. Cleland, and J. M. Martinis, Physical Review Letters **113** (2014), 10.1103/physrevlett.113.220502.
[172] P. Roushan, C. Neill, A. Megrant, Y. Chen, R. Babbush, R. Barends, B. Campbell, Z. Chen, B. Chiaro, A. Dunsworth, A. Fowler, E. Jeffrey, J. Kelly, E. Lucero, J. Mutus, P. J. J. O'Malley, M. Neeley, C. Quintana, D. Sank, A. Vainsencher, J. Wenner, T. White, E. Kapit, H. Neven, and J. Martinis, Nature Physics **13**, 146 (2017).
[173] A. Bermudez, T. Schaetz, and D. Porras, Phys. Rev. Lett. **107**, 150501 (2011).
[174] P. Hauke, O. Tieleman, A. Celi, C. Ölschläger, J. Simonet, J. Struck, M. Weinberg, P. Windpassinger, K. Sengstock, M. Lewenstein, and A. Eckardt, Phys. Rev. Lett. **109**, 145301 (2012).
[175] M. Aidelsburger, M. Atala, M. Lohse, J. T. Barreiro, B. Paredes, and I. Bloch, Phys. Rev. Lett. **111**, 185301 (2013).
[176] H. Miyake, G. A. Siviloglou, C. J. Kennedy, W. C. Burton, and W. Ketterle, Phys. Rev. Lett. **111**, 185302 (2013).
[177] M. Atala, M. Aidelsburger, M. Lohse, J. T. Barreiro, B. Paredes, and I. Bloch, Nature Physics **10**, 588 (2014).
[178] M. Aidelsburger, M. Lohse, C. Schweizer, M. Atala, J. T. Barreiro, S. Nascimbène, N. R. Cooper, I. Bloch, and N. Goldman, Nature Physics **11**, 162 (2015).
[179] N. A. Estep, D. L. Sounas, J. Soric, and A. Alù, Nature Physics **10**, 923 (2014).
[180] P. Kiefer, F. Hakelberg, M. Wittemer, A. Bermúdez, D. Porras, U. Warring, and T. Schaetz, Phys. Rev. Lett. **123**, 213605 (2019).
[181] J. Koch, A. A. Houck, K. L. Hur, and S. M. Girvin, Phys. Rev. A **82**, 043811 (2010).
[182] M. Hafezi, E. A. Demler, M. D. Lukin, and J. M. Taylor, Nature Physics **7**, 907 (2011).
[183] M. Hafezi, S. Mittal, J. Fan, A. Migdall, and J. M. Taylor, Nature Photonics **7**, 1001 (2013).
[184] S. Mittal, J. Fan, S. Faez, A. Migdall, J. M. Taylor, and M. Hafezi, Phys. Rev. Lett. **113**, 087403 (2014).
[185] S. Mittal, E. A. Goldschmidt, and M. Hafezi, Nature **561**, 502 (2018).
[186] T. Manovitz, Y. Shapira, N. Akerman, A. Stern, and R. Ozeri, PRX Quantum **1**, 020303 (2020).
[187] Y. Shapira, T. Manovitz, N. Akerman, A. Stern, and R. Ozeri, "Quantum simulations of interacting systems with broken time-reversal symmetry," (2022).
[188] M. A. Nielsen and I. L. Chuang, *Quantum Computation and Quantum Information* (Cambridge University Press, 2000).
[189] C. Gattringer and C. B. Lang, *Quantum chromodynamics on the lattice: an introductory presentation* (Springer, 2010).
[190] P. A. M. Dirac, Proceedings of the Royal Society of London. Series A, Containing Papers of a Mathematical and Physical Character **133**, 60 (1931).
[191] I. I. Rabi, Phys. Rev. **51**, 652 (1937).
[192] L. Allen and J. H. Eberly, *Optical resonance and two-level atoms*, Vol. 28 (Courier Corporation, 1987).
[193] E. Arimondo and G. Orriols, Lettere al Nuovo Cimento (1971-1985) **17**, 333 (1976).
[194] E. Arimondo (Elsevier, 1996) pp. 257–354.
[195] F. Benatti, R. Floreanini, F. Franchini, and U. Marzolino, Physics Reports **878**, 1 (2020), entanglement in indistinguishable particle systems.
[196] B. C. Sanders, Phys. Rev. A **40**, 2417 (1989).
[197] J. J. . Bollinger, W. M. Itano, D. J. Wineland, and D. J. Heinzen, Phys. Rev. A **54**, R4649 (1996).
[198] A. N. Boto, P. Kok, D. S. Abrams, S. L. Braunstein, C. P. Williams, and J. P. Dowling, Phys. Rev. Lett. **85**, 2733 (2000).
[199] H. Lee, P. Kok, and J. P. Dowling, Journal of Modern Optics **49**, 2325 (2002), https://doi.org/10.1080/0950034021000011536.
[200] V. Giovannetti, S. Lloyd, and L. Maccone, Nature Photonics **5**, 222 (2011).
[201] C. K. Hong, Z. Y. Ou, and L. Mandel, Phys. Rev. Lett. **59**,

2044 (1987).
[202] D. Leibfried, B. DeMarco, V. Meyer, M. Rowe, A. Ben-Kish, J. Britton, W. M. Itano, B. Jelenković, C. Langer, T. Rosenband, and D. J. Wineland, Phys. Rev. Lett. **89**, 247901 (2002).
[203] R. T. Sutherland and R. Srinivas, Phys. Rev. A **104**, 032609 (2021).
[204] C. Muschik, M. Heyl, E. Martinez, T. Monz, P. Schindler, B. Vogell, M. Dalmonte, P. Hauke, R. Blatt, and P. Zoller, New Journal of Physics **19**, 103020 (2017).
[205] Z. Davoudi, M. Hafezi, C. Monroe, G. Pagano, A. Seif, and A. Shaw, Phys. Rev. Research **2**, 023015 (2020).
[206] D. Paulson, L. Dellantonio, J. F. Haase, A. Celi, A. Kan, A. Jena, C. Kokail, R. van Bijnen, K. Jansen, P. Zoller, and C. A. Muschik, PRX Quantum **2**, 030334 (2021).
[207] E. J. Gustafson and H. Lamm, Phys. Rev. D **103**, 054507 (2021).
[208] L. Lumia, P. Torta, G. B. Mbeng, G. E. Santoro, E. Ercolessi, M. Burrello, and M. M. Wauters, PRX Quantum **3**, 020320 (2022).
[209] M. Carena, H. Lamm, Y.-Y. Li, and W. Liu, Phys. Rev. Lett. **129**, 051601 (2022).
[210] J. Mildenberger, W. Mruczkiewicz, J. C. Halimeh, Z. Jiang, and P. Hauke, "Probing confinement in a $\mathbb{Z}_2$ lattice gauge theory on a quantum computer," (2022).
[211] T. Greenberg, G. Pardo, A. Fortinsky, and E. Zohar, "Resource-efficient quantum simulation of lattice gauge theories in arbitrary dimensions: Solving for gauss' law and fermion elimination," (2022).
[212] R. Irmejs, M. C. Banuls, and J. I. Cirac, "Quantum simulation of z2 lattice gauge theory with minimal requirements," (2022).
[213] P. Hauke, D. Marcos, M. Dalmonte, and P. Zoller, Phys. Rev. X **3**, 041018 (2013).
[214] B. Andrade, Z. Davoudi, T. Graß, M. Hafezi, G. Pagano, and A. Seif, Quantum Science and Technology **7**, 034001 (2022).
[215] A. Bermudez, D. Porras, and M. A. Martin-Delgado, Phys. Rev. A **79**, 060303 (2009).
[216] O. Katz, M. Cetina, and C. Monroe, Phys. Rev. Lett. **129**, 063603 (2022).
[217] O. Katz, L. Feng, A. Risinger, C. Monroe, and M. Cetina, "Demonstration of three- and four-body interactions between trapped-ion spins," (2022).
[218] D. Yang, G. S. Giri, M. Johanning, C. Wunderlich, P. Zoller, and P. Hauke, Phys. Rev. A **94**, 052321 (2016).
[219] Z. Davoudi, N. M. Linke, and G. Pagano, Phys. Rev. Research **3**, 043072 (2021).
[220] P.-Y. Hou, J. J. Wu, S. D. Erickson, D. C. Cole, G. Zarantonello, A. D. Brandt, A. C. Wilson, D. H. Slichter, and D. Leibfried, "Coherently coupled mechanical oscillators in the quantum regime," (2022).
[221] R. T. Sutherland and R. Srinivas, Phys. Rev. A **104**, 032609 (2021).
[222] O. Katz and C. Monroe, "Programmable quantum simulations of bosonic systems with trapped ions," (2022).
[223] W. Chen, Y. Lu, S. Zhang, K. Zhang, G. Huang, M. Qiao, X. Su, J. Zhang, J.-N. Zhang, L. Banchi, M. S. Kim, and K. Kim, Nature Physics (2023), 10.1038/s41567-023-01952-5.
[224] D. Wineland, C. Monroe, W. Itano, D. Leibfried, B. King, and D. Meekhof, Reviews of Modern Physics (1998).
[225] D. Leibfried, B. DeMarco, V. Meyer, D. Lucas, M. Barrett, J. Britton, W. M. Itano, B. Jelenković, C. Langer, T. Rosenband, *et al.*, Nature **422**, 412 (2003).
[226] D. J. Wineland, M. Barrett, J. Britton, J. Chiaverini, B. DeMarco, W. M. Itano, B. Jelenković, C. Langer, D. Leibfried, V. Meyer, T. Rosenband, and T. Schätz, Philosophical Transactions of the Royal Society of London. Series A: Mathematical, Physical and Engineering Sciences **361**, 1349 (2003).
[227] H. C. J. Gan, G. Maslennikov, K.-W. Tseng, C. Nguyen, and D. Matsukevich, Phys. Rev. Lett. **124**, 170502 (2020).
[228] V. Schafer, *Fast gates and mixed-species entanglement with trapped ions*, Ph.D. thesis, University of Oxford (2018).
[229] K. Thirumalai, *High-fidelity mixed species entanglement of trapped ions*, Ph.D. thesis, University of Oxford (2019).
[230] S. Krämer, D. Plankensteiner, L. Ostermann, and H. Ritsch, Computer Physics Communications **227**, 109 (2018).
[231] A. Sørensen and K. Mølmer, Phys. Rev. Lett. **82**, 1971 (1999).
[232] K. Mølmer and A. Sørensen, Phys. Rev. Lett. **82**, 1835 (1999).
[233] A. Sørensen and K. Mølmer, Phys. Rev. A **62**, 022311 (2000).
[234] C. D. Bruzewicz, J. Chiaverini, R. McConnell, and J. M. Sage, Applied Physics Reviews **6**, 021314 (2019), https://doi.org/10.1063/1.5088164.
[235] W. Magnus, Communications on pure and applied mathematics **7**, 649 (1954).
[236] D. Leibfried, R. Blatt, C. Monroe, and D. Wineland, Rev. Mod. Phys. **75**, 281 (2003).
[237] D. J. Wineland, C. Monroe, W. M. Itano, D. Leibfried, B. E. King, and D. M. Meekhof, J. Res. Natl. Inst. Stand. Technol. **103**, 259 (1998).
[238] Light shifts can be created using quadrupole-Raman transitions [**?**] but extra care needs to be taken to symmetrise the shift induced on each qubit state.
[239] K. G. Johnson, J. D. Wong-Campos, A. Restelli, K. A. Landsman, B. Neyenhuis, J. Mizrahi, and C. Monroe, Review of Scientific Instruments **87** (2016), 10.1063/1.4948734, 053110, https://pubs.aip.org/aip/rsi/article-pdf/doi/10.1063/1.4948734/15778092/053110_1_online.pdf.
[240] L. Barbiero, C. Schweizer, M. Aidelsburger, E. Demler, N. Goldman, and F. Grusdt, Science Advances **5** (2019), 10.1126/sciadv.aav7444.
[241] A. Bermudez and D. Porras, New Journal of Physics **17**, 103021 (2015).
[242] R. Desbuquois, M. Messer, F. Görg, K. Sandholzer, G. Jotzu, and T. Esslinger, Phys. Rev. A **96**, 053602 (2017).
[243] F. Görg, K. Sandholzer, J. Minguzzi, R. Desbuquois, M. Messer, and T. Esslinger, Nature Physics **15**, 1161 (2019).
[244] A. Steane, Applied Physics B **64**, 623 (1997).
[245] D. F. V. James, Applied Physics B **66**, 181 (1998).
[246] C. Marquet, F. Schmidt-Kaler, and D. F. V. James, Applied Physics B **76**, 199 (2003).
[247] J. Chiaverini, R. B. Blakestad, J. Britton, J. D. Jost, C. Langer, D. Leibfried, R. Ozeri, and D. J. Wineland, "Surface-electrode architecture for ion-trap quantum information processing," (2005).
[248] C. E. Pearson, D. R. Leibrandt, W. S. Bakr, W. J. Mallard, K. R. Brown, and I. L. Chuang, Phys. Rev. A **73**, 032307 (2006).
[249] S. Seidelin, J. Chiaverini, R. Reichle, J. J. Bollinger, D. Leibfried, J. Britton, J. H. Wesenberg, R. B. Blakestad, R. J. Epstein, D. B. Hume, W. M. Itano, J. D. Jost, C. Langer, R. Ozeri, N. Shiga, and D. J. Wineland, Phys. Rev. Lett. **96**, 253003 (2006).
[250] J. Chiaverini and W. E. Lybarger, Phys. Rev. A **77**, 022324 (2008).
[251] J. Labaziewicz, Y. Ge, P. Antohi, D. Leibrandt, K. R. Brown, and I. L. Chuang, Phys. Rev. Lett. **100**, 013001 (2008).
[252] R. Schmied, J. H. Wesenberg, and D. Leibfried, Phys. Rev. Lett. **102**, 233002 (2009).

[253] M. Kumph, M. Brownnutt, and R. Blatt, New Journal of Physics **13**, 073043 (2011).
[254] J. Welzel, A. Bautista-Salvador, C. Abarbanel, V. Wineman-Fisher, C. Wunderlich, R. Folman, and F. Schmidt-Kaler, The European Physical Journal D **65**, 285 (2011).
[255] R. C. Sterling, H. Rattanasonti, S. Weidt, K. Lake, P. Srinivasan, S. C. Webster, M. Kraft, and W. K. Hensinger, Nature Communications **5**, 3637 (2014).
[256] M. Mielenz, H. Kalis, M. Wittemer, F. Hakelberg, U. Warring, R. Schmied, M. Blain, P. Maunz, D. L. Moehring, D. Leibfried, and T. Schaetz, Nature Communications **7**, ncomms11839 (2016).
[257] C. D. Bruzewicz, R. McConnell, J. Chiaverini, and J. M. Sage, Nature Communications **7**, 13005 (2016).
[258] M. Kumph, P. Holz, K. Langer, M. Meraner, M. Niedermayr, M. Brownnutt, and R. Blatt, New Journal of Physics **18**, 023047 (2016).
[259] S. Jain, J. Alonso, M. Grau, and J. P. Home, Phys. Rev. X **10**, 031027 (2020).
[260] F. Hebenstreit, J. Berges, and D. Gelfand, Phys. Rev. Lett. **111**, 201601 (2013).
[261] S. Kuehn, P. Sala, T. Shi, M. C. Banuls, E. Demler, and J. I. Cirac, in *Proceedings of The 36th Annual International Symposium on Lattice Field Theory — PoS(LATTICE2018)* (Sissa Medialab, 2019).
[262] T. Chanda, J. Zakrzewski, M. Lewenstein, and L. Tagliacozzo, Phys. Rev. Lett. **124**, 180602 (2020).
[263] G. H. Wannier, Rev. Mod. Phys. **34**, 645 (1962).
[264] H. Fukuyama, R. A. Bari, and H. C. Fogedby, Phys. Rev. B **8**, 5579 (1973).
[265] M. Grifoni and P. Hänggi, Physics Reports **304**, 229 (1998).
[266] M. Holthaus and D. W. Hone, Philosophical Magazine B **74**, 105 (1996), https://doi.org/10.1080/01418639608240331.
[267] T. Hartmann, F. Keck, H. J. Korsch, and S. Mossmann, New Journal of Physics **6**, 2 (2004).
[268] U. Schollwöck, Annals of physics **326**, 96 (2011).
[269] R. Orús, Annals of Physics **349**, 117 (2014).
[270] S. R. White, Physical review letters **69**, 2863 (1992).
[271] G. Vidal, Physical review letters **91**, 147902 (2003).
[272] S. Paeckel, T. Köhler, A. Swoboda, S. R. Manmana, U. Schollwöck, and C. Hubig, Annals of Physics **411**, 167998 (2019).
[273] J. Haegeman, J. I. Cirac, T. J. Osborne, I. Pižorn, H. Verschelde, and F. Verstraete, Physical review letters **107**, 070601 (2011).
[274] J. Haegeman, C. Lubich, I. Oseledets, B. Vandereycken, and F. Verstraete, Physical Review B **94**, 165116 (2016).
[275] N. Mott and W. Twose, Advances in Physics **10**, 107 (1961), https://doi.org/10.1080/00018736100101271.
[276] A. Bermudez, M. A. Martin-Delgado, and D. Porras, New Journal of Physics **12**, 123016 (2010).
[277] M. P. A. Fisher, P. B. Weichman, G. Grinstein, and D. S. Fisher, Phys. Rev. B **40**, 546 (1989).
[278] M. Valiente and D. Petrosyan, Europhysics Letters **83**, 30007 (2008).
[279] M. Valiente, Phys. Rev. A **81**, 042102 (2010).
[280] C. D. E. Boschi, E. Ercolessi, L. Ferrari, P. Naldesi, F. Ortolani, and L. Taddia, Phys. Rev. A **90**, 043606 (2014).
[281] B. Buyens, J. Haegeman, F. Hebenstreit, F. Verstraete, and K. Van Acoleyen, Phys. Rev. D **96**, 114501 (2017).
[282] P. Sala, T. Shi, S. Kühn, M. C. Bañuls, E. Demler, and J. I. Cirac, Phys. Rev. D **98**, 034505 (2018).
[283] A. Florio, D. Frenklakh, K. Ikeda, D. Kharzeev, V. Korepin, S. Shi, and K. Yu, Phys. Rev. Lett. **131**, 021902 (2023).
[284] I. Papaefstathiou, J. Knolle, and M. C. Bañuls, "Real-time scattering in the lattice schwinger model," (2024), arXiv:2402.18429 [hep-lat].
[285] G.-X. Su, J. Osborne, and J. C. Halimeh, "A cold-atom particle collider," (2024), arXiv:2401.05489 [cond-mat.quant-gas].
[286] J. Schwinger, Phys. Rev. **82**, 664 (1951).
[287] R. Peierls, Zeitschrift für Physik **80**, 763 (1933).
[288] D. R. Hofstadter, Phys. Rev. B **14**, 2239 (1976).
[289] D. J. Thouless, M. Kohmoto, M. P. Nightingale, and M. den Nijs, Phys. Rev. Lett. **49**, 405 (1982).
[290] M. G. Raizen, J. M. Gilligan, J. C. Bergquist, W. M. Itano, and D. J. Wineland, Phys. Rev. A **45**, 6493 (1992).
[291] D. Porras and J. I. Cirac, Phys. Rev. Lett. **93**, 263602 (2004).
[292] D. J. Berkeland, J. D. Miller, J. C. Bergquist, W. M. Itano, and D. J. Wineland, Journal of Applied Physics **83**, 5025 (1998), https://doi.org/10.1063/1.367318.
[293] A. Bermudez, P. Schindler, T. Monz, R. Blatt, and M. Müller, New Journal of Physics **19**, 113038 (2017).
[294] G. Martín-Vázquez, G. Aarts, M. Müller, and A. Bermudez, PRX Quantum **3**, 020352 (2022).
[295] K. R. Brown, C. Ospelkaus, Y. Colombe, A. C. Wilson, D. Leibfried, and D. J. Wineland, Nature **471**, 196 (2011).
[296] M. Harlander, R. Lechner, M. Brownnutt, R. Blatt, and W. Hänsel, Nature **471**, 200 (2011).
[297] A. C. Wilson, Y. Colombe, K. R. Brown, E. Knill, D. Leibfried, and D. J. Wineland, Nature **512**, 57 (2014).
[298] M. Ramm, T. Pruttivarasin, and H. Häffner, New Journal of Physics **16**, 063062 (2014).
[299] K. Toyoda, R. Hiji, A. Noguchi, and S. Urabe, Nature **527**, 74 (2015).
[300] S. Debnath, N. M. Linke, S.-T. Wang, C. Figgatt, K. A. Landsman, L.-M. Duan, and C. Monroe, Phys. Rev. Lett. **120**, 073001 (2018).
[301] F. Hakelberg, P. Kiefer, M. Wittemer, U. Warring, and T. Schaetz, Phys. Rev. Lett. **123**, 100504 (2019).
[302] M. Tamura, T. Mukaiyama, and K. Toyoda, Phys. Rev. Lett. **124**, 200501 (2020).
[303] D. J. Heinzen and D. J. Wineland, Phys. Rev. A **42**, 2977 (1990).
[304] E. A. Cornell, R. M. Weisskoff, K. R. Boyce, and D. E. Pritchard, Phys. Rev. A **41**, 312 (1990).
[305] D. M. Meekhof, C. Monroe, B. E. King, W. M. Itano, and D. J. Wineland, Phys. Rev. Lett. **76**, 1796 (1996).
[306] S. C. Burd, R. Srinivas, J. J. Bollinger, A. C. Wilson, D. J. Wineland, D. Leibfried, D. H. Slichter, and D. T. C. Allcock, Science **364**, 1163 (2019).
[307] A similar argument can be made for a qubit encoding formed by two sub-levels of a metastable manifold.
[308] A. Noguchi, Y. Shikano, K. Toyoda, and S. Urabe, Nature Communications **5**, 3868 (2014).
[309] G.-D. Lin, S.-L. Zhu, R. Islam, K. Kim, M.-S. Chang, S. Korenblit, C. Monroe, and L.-M. Duan, Europhysics Letters **86**, 60004 (2009).
[310] Y. Xie, X. Zhang, B. Ou, T. Chen, J. Zhang, C. Wu, W. Wu, and P. Chen, Phys. Rev. A **95**, 032341 (2017).
[311] M. Johanning, Applied Physics B **122**, 71 (2016).
[312] P. H. Leung and K. R. Brown, Phys. Rev. A **98**, 032318 (2018).
[313] G. Pagano, P. W. Hess, H. B. Kaplan, W. L. Tan, P. Richerme, P. Becker, A. Kyprianidis, J. Zhang, E. Birckelbaw, M. R. Hernandez, Y. Wu, and C. Monroe, Quantum Science and Technology **4**, 014004 (2018).
[314] H.-K. Li, E. Urban, C. Noel, A. Chuang, Y. Xia, A. Ransford, B. Hemmerling, Y. Wang, T. Li, H. Häffner, and X. Zhang,

Phys. Rev. Lett. **118**, 053001 (2017).
[315] E. Urban, N. Glikin, S. Mouradian, K. Krimmel, B. Hemmerling, and H. Haeffner, Phys. Rev. Lett. **123**, 133202 (2019).
[316] G. Martínez-Carracedo, MSc Thesis, Universidad Complutense de Madrid (2019).
[317] C. F. Roos, New Journal of Physics **10**, 013002 (2008).
[318] O. Katz, L. Feng, A. Risinger, C. Monroe, and M. Cetina, "Demonstration of three- and four-body interactions between trapped-ion spins," (2022).
[319] O. Katz, M. Cetina, and C. Monroe, "Programmable n-body interactions with trapped ions," (2022).
[320] F. Domínguez-Adame, European Journal of Physics **31**, 639 (2010).
[321] P. W. Anderson, Phys. Rev. **109**, 1492 (1958).
[322] A. Gray, E. Gray, G. B. Mathews, and E. Meissel, *A treatise on Bessel functions and their applications to physics* (Macmillan and Company, 1895).